TITLE:

Dynamic stress- and inflammatory-based regulation of psychiatric risk loci in human neurons

AUTHORS:

Kayla G. Retallick-Townsley[1-2,4], Seoyeon Lee[5,6], Sam Cartwright[1,4*], Sophie Cohen[1,4*], Annabel Sen[5,6*], Meng Jia[5,6], Hannah Young[1,3], Lee Dobbyn[1-3], Michael Deans[5,6], Meilin Fernandez-Garcia[5,6], Laura M. Huckins[5#], Kristen J. Brennand[1,4,5,6#]

AFFILIATIONS

[1]Department of Genetics and Genomics, Icahn School of Medicine at Mount Sinai, New York, NY, USA.

[2]Icahn Institute of Genomics and Multiscale Biology, Icahn School of Medicine at Mount Sinai, New York, NY, USA.

[3]Pamela Sklar Division of Psychiatric Genomics, Icahn School of Medicine at Mount Sinai, New York, NY, USA.

[4] Nash Family Department of Neuroscience, Friedman Brain Institute, Icahn School of Medicine at Mount Sinai, New York, NY 10029

[5] Department of Psychiatry, Division of Molecular Psychiatry, Yale University School of Medicine, New Haven, CT 06511

[6] Department of Genetics, Wu Tsai Institute, Yale University School of Medicine, New Haven, CT 06511

*Contributed equally

#Co-corresponence: kristen.brennand@yale.edu and laura.huckins@yale.edu

ABSTRACT

The prenatal environment can alter neurodevelopmental and clinical trajectories, markedly increasing risk for psychiatric disorders in childhood and adolescence. To understand if and how fetal exposures to stress and inflammation exacerbate manifestation of genetic risk for complex brain disorders, we report a large-scale context-dependent massively parallel reporter assay (MPRA) in human neurons designed to catalogue genotype x environment (GxE) interactions. Across 240 genome-wide association study (GWAS) loci linked to ten brain traits/disorders, the impact of hydrocortisone, interleukin 6, and interferon alpha on transcriptional activity is empirically evaluated in human induced pluripotent stem cell (hiPSC)-derived glutamatergic neurons. Of ~3,500 candidate regulatory risk elements (CREs), 11% of variants are active at baseline, whereas cue-specific CRE regulatory activity range from a high of 23% (hydrocortisone) to a low of 6% (IL-6). Cue-specific regulatory activity is driven, at least in part, by differences in transcription factor binding activity, the gene targets of which show unique enrichments for brain disorders as well as co-morbid metabolic and immune syndromes. The dynamic nature of genetic regulation informs the influence of environmental factors, reveals a mechanism underlying pleiotropy and variable penetrance, and identifies specific risk variants that confer greater disorder susceptibility after exposure to stress or inflammation. Understanding neurodevelopmental GxE interactions will inform mental health trajectories and uncover novel targets for therapeutic intervention.

KEYWORDS

MPRA, context-specific expression quantitative trait loci, psychiatric genetics, stress and inflammation, fetal brain development

Introduction

Genome-wide association studies (GWAS) identified hundreds of significant loci associated with psychiatric[9-12] and neurodegenerative disease risk[13,14]. The overwhelming majority of these risk loci are comprised of variants that are non-coding, common in the population at large, and thought to confer heightened risk by regulating the expression of one or more target genes (eGenes)[1,2,16]. Critically, the weighted sum of all GWAS risk alleles falls short of explaining phenotypic variance and does not predict individual outcomes[3], suggesting that additional factors may underlie the penetrance and expressivity of genetic risk for complex brain disorders. For example, immune signaling and stress, particularly fetal exposures, are well-established environmental risk factors associated with psychiatric disorders. Although the causal mechanisms involved remain unresolved, maternal immune activation (MIA) induces pro-inflammatory agents and neuropoietic cytokines, circulating levels of which alter the release of glucocorticoids from the adrenal gland[4,5]. Maternal cytokines and steroid hormones cross the placental barrier and reach the fetal vasculature and brain[6,7], where they impact gene expression and neurodevelopment[8,9,10] *in vivo,* effects that are recapitulated in a dose-dependent manner *in vitro*[11,12]. Interaction of cytokines in the developing brain with risk-associated regulatory elements may explain, in part, how fetal exposures increase risk for brain disorders in offspring.

Genomic analyses typically yield static predictions of gene expression derived from post-mortem analyses, predicting genetic regulation at baseline. If, however, the regulatory activity of non-coding risk variants is indeed influenced by environmental interactions, context-specific influences of the regulome could shape risk for brain disorders. Consistent with this, genetic loci that explain variation in expression levels of mRNAs (termed expression quantitative trait loci, "eQTL") differ between tissues[13–15], cell-types[16–18], and sexes[19–21]. eQTLs are likewise dynamically regulated (e.g. by immune[22,23] and stress[24–26] signaling); notably, these changes in regulatory activity also occur in a cell-type specific manner[27,28]. Nonetheless, to date, nearly all evidence of context-dependent genetic regulation reflects studies of blood cells only. Here we describe the mechanisms by which regulatory sequences result in distinct patterns of neuronal gene expression across stress and inflammatory cues.

To test the hypothesis that environmental effects interact with putative regulatory elements to mediate gene expression and impact risk for psychiatric disorders, we characterized thousands of GWAS loci in neurons *en masse.* Coupling massively parallel reporter assays (MPRAs)[29–32] with human induced pluripotent stem cell (hiPSC) models makes it possible to empirically evaluate the regulation of transcriptional activity[33,34,35] in live human neurons[30,36]. We quantified dynamic psychiatric risk loci activity of 240 GWAS loci associated with ten complex brain psychiatric disorders and traits, totaling ~9,000 candidate regulatory risk elements (CREs), in neurons treated with glucocorticoids and cytokines associated with MIA [synthetic cortisol (hCort)[4,12,37], interleukin-6 (IL-6)[43–46], and interferon alfa-2b (IFNa-2b)[41,42]]. We uncovered GxE influences that altered the impact of distinct disorder-specific risk elements across contexts. Moreover, we described how stress- and inflammation-dynamic regulatory effects converge on downstream biology to impact shared risk for neuropsychiatric and neurodevelopmental disorders. Altogether, we modelled dynamic prenatal contributions to psychiatric risk that can precede symptom onset and disorder etiology by decades.

Results

Stress and inflammatory factors have shared and distinct neuronal impacts on cellular function and the transcriptome.

To assess the influence of stress and inflammatory cues on developing human neurons, hiPSC-derived *NGN2*-induced glutamatergic neurons (iGLUTs)[32,33] were acutely (48-hours) treated with hCort (1000nM), IL-6 (60ng/uL), or IFNa-2b (500 UI/mL). hCort significantly reduced neurite

outgrowth (D7) (p-value<0.001) and IFNa significantly increased neurite outgrowth (p-value<0.001) (**Figure 1j-k**). Exposure to hCort, IFNa, and IL6 did not affect neuronal survival (**Figure 1j-k**) or synaptic puncta density (D24) (**SI Figure 4**). Differential gene expression analysis revealed that hCort resulted in the greatest transcriptome-wide dysregulation (7332 down- and 5684 up-regulated differentially expressed genes (DEGs)) (FDR<0.05), with more modest effects resulting from IFNa-2b (25 down- and 80 up-regulated) and IL-6 (10 down-regulated genes) (**Figure 1A**). Reciprocally, chromatin accessibility changes were greatest with IL-6 (675 differentially active regions (DARs); FDR <=0.05), more modest with IFNa (12 DARs; FDR<=0.05) and not significant with hCort (**Figure 1D**).

Stress and inflammation DEGs (unadjusted p-value <=0.05) were enriched for GWAS risk genes across complex brain and immune disorders; each exposure revealed unique disease enrichment profiles (**SI Tables 1-2**). Beyond GWAS, there were shared and unique significant enrichments in genes associated with neurological, neurodegenerative, and neurocognitive disorders across exposures (**Supplemental Table 1-2**). Shared enrichments were occasionally predicted to have opposing effects—for example, while all cues were enriched for dementia, tauopathy, and Alzheimer's Disease (AD), hCort exposure decreased activity of these and related pathways [Alzheimer's disease; Alzheimer's disease or frontotemporal dementia; Degenerative dementia (FDR<=0.01, Activation z-score=-1); Dementia (FDR<=0.01, Activation z-score=-1.02); Tauopathy (FDR<=0.01, Activation z-score=-0.447)] and uniquely activated context memory (FDR<=0.01, Z=2.178).

Transcriptomic signatures following exposure to hCort, IL-6, and IFNa-2b resembled fetal expression signatures from four rodent models of MIA and prenatal stress: poly(I|C) (conceptus, whole brain, amygdala, and frontal cortex)[43,44,45], IL-6 (whole brain)[44], *H1N1* Flu virus (whole brain)[44], and chronic unpredictable maternal stress (whole brain)[46]. hCort, IFNa-2b, and IL-6 DEGs were correlated to (**Figure 1D-F**) and significantly enriched for (**Figure 1G**) MIA-induced DEGs across immunogens and tissues. Meta-analysis across contexts revealed convergent changes of gene expression in the same direction across all conditions: 258 genes down- and 352 genes were upregulated change (meta-analysis FDR<=0.05) (**SI Figure 3B**). Pathway analysis[47] contextualized the impact of nominally significant DEGs (unadjusted p-value<=0.05); for example, across exposures, DEGs were enriched for mTOR signaling [hCort(-log(p)=2.08, Z=-0.71); IFNa-2B(-log(p)=6.25, Z=0; IL-6(-log(p)=3.7, no activity pattern] and decreased oxidative phosphorylation pathways [hCort(-log(p)=1.32, Z=-3.4); IFNa-2B(-log(p)=6.66, Z=-4.9; IL-6(-log(p)=1.15, -3] (**SI Figure 3C**, **SI Table 2**), pathways associated with MIA and linked to neuronal survival and the regulation of synapse formation, growth, and survival.

Stress and inflammatory factors dynamically and specifically impacted allelic shifts in neuronal transcriptional activity.

We designed a Lenti-MPRA[31] library through statistical fine-mapping of ten psychiatric GWAS: Alzheimer's Disease (AD)[48], Attention Deficit hyper-Activity Disorder (ADHD)[49], Anorexia Nervosa (AN)[50], Autism spectrum disorder (ASD)[51], Bipolar Disorder (BIP)[52], Major Depressive Disorder (MDD)[53], Obsessive Compulsive Disorder (OCD)[54], Post traumatic stress disorder (PTSD)[55], and Schizophrenia (SCZ)[56], as well as quantitative measurement of the personality trait, neuroticism (NEU-P)[57] (**SI Table 1**) using two complimentary methods incorporating dorsolateral prefrontal cortex (DLPFC)[8] expression quantitative trait loci (eQTLs): Bayesian co-localization (coloc2[58,59]) and transcriptomic imputation (S-PrediXcan[60,61]) (**SI Figure 1-2; SI Table 1-3**). In total, from 240 GWAS loci, our Lenti-MPRA library included ~9,000 SNPs, represented as ~4,500 biallelic candidate regulatory elements (CREs).

Glutamatergic neuron promoter and enhancer regions[62] and gene expression[63] are highly enriched across multiple psychiatric and behavioral traits. MPRAs were performed in iGLUTs

induced from two control donors, with two biological replicates each, exposed to acute (48 hours) hCort (1000nM), IL-6 (100ng/mL), IFNa-2b (500 UI/mL), or matched vehicles, 24 hours following Lenti-MPRA transduction. Paired MPRAs in iGLUT neurons with or without exposure resolved the context-specific regulatory activity of 3400-3747 variants. Across MPRAs, activity between replicates and donors was highly correlated (**SI Figure 5-6**). At baseline, 11% of all captured CRE (N=363) were significantly (FDR<0.1) transcriptionally active compared to scramble sequences (**Figure 2A**), comparable to previous eQTL-based MPRAs[64]. Mean alpha transcriptional activity varied between cues [Fwelch (3,7805.15) =517.79, p<0.001, nObs=14,119], with hCort most increasing overall transcriptional activity (23% of CRE; N=850) (Games-Howell Pairwise comparison of hCort to baseline, Holm-adjusted p-value=2.43e-11) (**Figure 2B**), and IL-6 and baseline being most similar (rank-rank hypergeometric overlap (RRHO) across all CRE) (**Figure 2D**). The majority of top significant CRS were unique to each cue exposure (**Figure 2C; SI Fig 7**). Moreover, active CRE showed cue-specific enrichments for psychiatric disorder GWAS risk loci, despite each having the same proportion of tested CRS by prioritization GWAS (**Figure 2E**; **SI Figure 6**).

A single variant change frequently influenced dynamic regulatory activity, with significant allelic shifts between baseline and IL-6 (10% CRE), hCort (9%), or IFNa-2b (4%) (**Figure 2A**;)**.** Most of these allelic shifts were context-specific (**Figure 2, SI Figure 7**). These allelic-shifts recapitulated eQTL effects, with allelic shifts significantly positively associated (FDR<0.05) with single-cell brain eQTLs[16] (baseline, IFNa, hCort) and fetal brain eQTLs[65] (baseline, IFNa). Notably, allelic shifts across all conditions were negatively associated with adult DLPFC eQTLs, significantly so at baseline and following hCort exposure (**Figure 2Fi-ii**).

CTCF binding negatively influenced transcriptional activity in a cue-specific manner.

The majority of active CRE identified by MPRA were novel and not previously annotated (**Figure 3A**). Baseline MPRA CRE activity was inversely associated with binding of CCCTC-binding factor (CTCF), with active CREs disproportionately overlapping non-CTCF bound enhancers (**SI Figure 9A**), and non-CTCF-bound sequences having significantly higher average activity of than CTCF-bound regions (**SI Figure 9B**). There was likewise a nominally significant negative relationship with annotated CTCF binding sites and transcriptional activity (linear correlation coefficient = -0.25, unadjusted p-value<=0.05) (**Figure 3B**). Quantitative CTCF motif binding scores across highly conserved motifs [FDR<0.05 (LM23, REN20); unadjusted P<0.05 (LM2, LM7)] revealed negative associations with transcriptional activity at baseline (**Figure 3Bi-ii**).

Conversely, stress and inflammatory MPRA CRE activity was more likely to be CTCF-independent and/or mediated by CTCF interactions distinct from those identified at baseline. There was a significant positive association between a lack of CTCF-binding and transcriptional activity following IL-6 exposure (linear correlation coefficient = 0.3, FDR<=0.05) (**Figure 3B**), although the proportion of active CRE overlapping with non-CTCF-bound enhancers still exceeded CTCF-bound enhancer-like sequences (**SI Figure 9A**). CTCF expression was significantly downregulated following hCort, and a unique CTCF motif (M1) was nominally positively associated with hCort-responsive transcriptional activity (**Figure 3Ci-ii**).

While CTCF binding may partially mediate cue-specific genetically regulated expression of brain disorder risk loci, only a subset of the CRE overlapping with annotated CTCF binding regions genome-wide (n=~220-250) were significantly active by MPRA (n=18-60). Thus, we next sought to resolve additional transcriptional regulators mediating dynamic regulation of gene expression.

Risk variants disrupted transcription factor binding to underly GxE specific activity.

Direct comparative analysis of transcriptional activity revealed cue-by-variant specific effects (**Figure 4A-C**); many CREs showed disproportionately increased activity relative to baseline

(hCort: 166 nominally significant CRE (p<0.05) showed increased activity, 25 decreased activity; IL-6: 95 increased, 41 decreased; IFNa-2b: 97 increased, 37 decreased). Altogether, 45 CREs were consistently up-regulated and 11 down-regulated across all cues (**Figure 4F**). The top significant GWAS-risk enrichments of differentially active allele-specific CREs differed by exposure, with non-specific psychiatric enrichments for hCort (ASD FDR=1.2e-03; ratio=15.5; CxD FDR=6.8-03, ratio=1.75; SCZ FDR= 1.04e-02, ratio=1.3) and IFNa-2b (ASD FDR=5.4e-03; ratio=13.7; CxD FDR=1.7e-03, ratio=1.98; SCZ FDR=5.4e-03,ratio=1.4) and more specific ASD/ADHD enrichments strongest for IL-6 (ASD FDR=1.49e-05; enrichment ratio=24.5; ADHD FDR=1.07e-02; ratio=7.4) (**Figure 4D**).

Given the dysregulation of transcription factor (TF) expression following stress and inflammatory exposures (**SI Figures 8,11**), we speculated that TFs mediate cue-specific genetic regulation of gene expression. Motif enrichment analysis indeed uncovered shared and unique TF binding motifs for significantly active CRE across exposures, many of which were TFs differentially expressed between exposures (**SI Figure 8)**. To identify the top TFs most likely to have variant specific binding across CREs, allele-specific TF binding affinities centered at the variant of interest were resolved using local differential enrichment for known motifs (CentriMo[66]) (**SI Figure 8**). MXI1, POU3F2, and AHR binding motifs were uniquely differentially enriched in IL-6, IFNa-2b, and hCort respectively; ARNT and EPAS were differentially enriched across all cues. Many enriched TFs were associated with complex brain disorders, infection, and autoimmune disease[67] and tended to be important for neurodevelopment and/or neuron-specific (**SI Figure 8**). We further explored cue-by-variant specific regulation for top differentially active regulatory elements individually (MotifBreaker[68]), identifying multiple CREs were binding affinity of TFs with cue-dynamic expression differed between the alternative and reference alleles. (**Figure 4E**).

MPRA TF affinity binding patterns with variant-specific transcriptional activity were predicted using differential TF binding affinity prediction scores (deltaSVM[69–71]) (**Figure 4Bi; Figure 5A**;**T SI Figure 8**), revealing a significant association of cue-specific allelic shifts (**Figure 5Bii)**, with distinct TFs across exposures (**Figure 5C**). Top TFs were enriched for neurogenesis (FDR=8.06e-3), forebrain development (FDR=3.37e-2), and neural crest differentiation (FDR=8.58e-4) and many were previously linked to risk across complex brain disorders. For example, *CUX1*, *ESRRG*, *HLF*, *SCRT1* are primary targets of has-miR-137 (FDR<0.05) – a key miRNA regulating expression of SCZ risk genes. *LHX6* and *SPIB,* and *ELK1* and *RFX2,* are targets of primary non-synonymous SCZ and ASD rare variants, respectively and *YY2* has been previously implicated in the regulation of PTSD risk.

Gene targets of context-specific regulatory elements showed distinct associations with brain disorders.

Target genes directly regulated by cue-specific genetic regulation were predicted using an adapted activity-by-contact (ABC[79]) model that incorporates TF binding affinities (STARE[72,73]), thereby integrating dynamic MPRA and cue-specific chromatin peak calls in matched iGLUTs. Shared and unique cue-specific gene targets were identified across contexts (**Figure 6A-B),** revealing significant overlap between enhancer-to-gene mapping (ABC) and the original eGene predictions (S-PrediXcan and Coloc2) (**Table 1**). Across all MPRA CREs, 5157 unique ABC genes with high interaction scores (ABC score >=0.8) were identified, 95 of which were amongst the 168 eGenes predicted by S-PrediXcan/Coloc2 that were also expressed in iGLUTs (hypergeometric test for enrichment, p-vale=1.5e-16) (**Table 1**). ABC genes and eGenes were found in cue-responsive DEGs; 45 DEGs were both (hypergeometric test; p-value=1.9e-8) (**Table 1**). Whereas *FURIN*, associated with BIP and SCZ, or *AP2A2,* associated with AD, were both predicted targets of active MPRA CREs at baseline only, *IRF2BP1*, *TOMM40,* and *EML2* were specifically predicted to be targets of IL-6-responsive CREs. Gene targets unique to cue-specific regulatory elements (ABC genes of active MPRAs CRE with differential activity between one or

more cues and baseline; FDR<=0.1) revealed unique gene ontology (GO) enrichments for proteasome complex pathways, clathrin coating, and the nuclear speck (hCort) and apical dendrite, G-protein alpha-subunit binding, and mitochondrial function (IL-6) and ganglion development and cytoplasmic translation (IFNa-2b) (**SI Figure 12**).

Cue-specific ABC gene targets were uniquely enriched for risk genes associated with complex brain disorders and common comorbid metabolic and immune syndromes (MAGMA[74]). For example, IFNa-2b-specific gene targets highlighted BIP sub-type II, whereas hCort was broadly linked to SCZ, BIP, and BIP sub-type I risk genes**,** and IL-6 to PTSD risk genes **(Figure 6C).** Likewise, shared and unique enrichments for neuropsychiatric, neurodegenerative, and emotional well-being, as well as allergy and autoimmune disorder-related GWAS risk genes, were revealed via over representation analysis across GWAS catalogue gene sets (FUMA[75]) **(Figure 6D).** ABC genes across all contexts were significantly enriched for SCZ, ASD, and AN, whereas IL-6 ABC genes were uniquely enriched in numerous measurements relating to Alzheimer's disease.

Drugs predicted to reverse cue-specific signatures in neural cells (defined as the z-scored ABC activity score of reference versus alternative alleles, using cMAP query tool[76]) and then filtered based on clinical trial phase included targets of glucocorticoid, androgen, and serotonin receptors, as well as drugs regulating inflammatory signaling (statins and non-steroidal anti-inflammatory drugs (NSAIDs)) (**Figure 6E**). Cue-specific signatures were reversed by drugs modulating serotonin – IFNa-specific signatures were reversed by treatment with serotonin itself while monoamine oxidase inhibiters (MOAIs) and the serotonin reuptake inhibitors (SSRIs) sertraline reversed hCort-specific and IL6-specifc transcriptomic signatures respectively. This highlights the importance of context in predicting targets of risk-associate genetic regulation and for precision pharmacology. Notably, FDA approved statins reversed the hCort-specific (atorvastatin) and INFa-specific (somatostatin) signatures, which is notable given that patients with SCZ, mood disorders, and AD often have reduced CSF (cerebral spinal fluid) and brain (DLPFC, hippocampus) somatostatin levels[77]. Somatostatin-positive interneurons are associated with cognitive deficits in schizophrenia[78], where adjunctive therapy with statins improved symptoms and cognition in SCZ patients[79,80].

Discussion

This work empirically annotated the functional impact of thousands of variants across hundreds of brain disorder GWAS loci, demonstrating that many variants could only be resolved under cue-responsive conditions. Treatment of human neurons with stress and inflammatory cues associated with prenatal exposures altered genetic regulation of expression of genes linked to a psychiatric and neurodegenerative conditions. From ~3,400 common-risk variants associated with ten complex brain disorders and traits, 10-11% were active at baseline and following IFNa exposure, while IL6 reduced overall transcriptional activity (6%) and hCort increased activity (23%). Across cues, MPRA validated risk-associated eQTLs and identifying novel regulatory elements—only 15% of tested CREs overlapped with annotated cCREs[81,82]; just 1-3% of annotated cCREs showed activity in our neuronal MPRAs, with active CRE not significantly enriched for annotated ENCODE cCREs[81,82]. This lack of overlap was observed in other studies and highlighted the importance of cell-type specificity[64]. The proportion of proximal or distal enhancer-like sequences in active MPRA CREs varied between contexts, suggesting a role for CCCTC-binding factor (CTCF) in cue-specific regulation; CTCF binds to DNA, forms chromatin loops, and regulates gene expression by promoting distal enhancer-dependent gene activation[83]. While CTCF binding was modestly negatively correlated with cue-specific activity at baseline, many TFs were strongly enriched for dynamic transcriptional regulation, with predicted potential downstream effects on neurodevelopment, synaptic plasticity, and immune response processes. As a simple example, expression of *PAX5*, a transcriptional activator and important regulator of

neurodevelopment[84,85] associated with multiple psychiatric traits[84,86,67], showed upregulated expression following IL-6 exposure, with IL-6-responsive CREs likewise enriched for the Pax5 motif. At the AD-associated *NDUFAF6* locus, PAX5 has decreased predicted binding affinity with the risk allele (rs28560301); IL6-exposure increased *PAX5* expression and significantly decreased risk allele activity (**Figure 4Ei-iii**). More complex co-regulation occurs at the *CNTN4* locus, where the SCZ-associated alternative allele (rs1719446) was significantly more active following hCort exposure: several transcriptional activators (CREB, CREM, ATF3) with increased binding affinities for the reference allele were significantly downregulated following hCort exposure; reciprocally, REST, a master transcriptional silencer, had increased binding to the risk allele and was also downregulated following hCort. Altogether, hCort-specific activity of this CRE may be mediated by both decreased expression of transcriptional activators and increased expression of transcriptional repressors, which showed differential allele-specific binding (**Figure 4Eiv-vi**). We posit that differential TF binding to risk-associated variants underlies dynamic GxE interactions, with cue-specific enrichments for psychiatric risk.

In modelling the GxE impact of maternal stress and inflammation *in utero,* we selected three MIA and psychiatric-risk associated immune molecules (IL6[43–46], IFNa-2b[41,42], and synthetic cortisol[4,12,37]) capable of transfer across blood brain barrier (BBB)[6,7] and modulation of the hypothalamic-pituitary-adrenal axis (HPA) signaling. The influence of pro-inflammatory environmental factors on brain-related regulatory elements may explain, in part, the biological mechanisms through which immune signaling contributes to increased susceptibility for complex brain disorders. Specifically, cytokine and glucocorticoid signaling can interact with genetic risk to mediate the genetically regulated gene expression[22,23,25,87,88], potentially contributing to the increased relative risk associated with stress and inflammation. Physiological and behavioral outcomes in rodent MIA models are sensitive to immunogen-type, exposure duration, and developmental timepoint[89]. Moreover, indirect mechanisms (e.g., changes to the microbiome) may facilitate immune activation and lead to alterations in brain-wide connectivity[90–92]. Therefore, the complexity and variability of human prenatal stress and rodent MIA are impossible to fully reproduce in a controlled *in vitro* model. Future MPRA incorporating longitudinal, repeated dosing, and recovery windows following exposure will be crucial for understanding how type, duration, and timing of immune activation during fetal development contributes to risk.

Developmental patterns of TF expression and enhancer activity may in part underly critical periods of heighted susceptibility to environmental stressors. Previous MPRAs identified time-point specific enhancers regulating neurodevelopment[30,36]. Likewise, temporally-dynamic and age-specific eQTLs highlight the importance of neurodevelopment and aging on genetically regulated gene expression[93–95]. Enhancer activity of regulatory elements tested in iGLUTs are significantly positively correlated with eQTL effect sizes from single cell data[16] and the fetal postmortem[65] brain, but, negatively correlated with adult DLPFC eQTLs[96]. Indeed, although stronger positive associations in fetal datasets relative to adult brain is not surprising, the reversal of the association supports the need to increase age-eQTL analyses. Age-eQTLs[16,95,97] modify the functional impact of genetic risk throughout life, particularly given the variable age of onset of symptom presentation across psychiatric disorders[98]. Previous studies have identified time-point specific enhancers regulating development of neuronal progenitor cells using MPRAs . It is likely that shifting developmental patterns of TF expression mediates temporal specific enhancer activity, contributing to critical periods of heighted susceptibility to environmental stressors. Thus, further exploration of the impact of shifting patterns of TF expression on age-eQTLs across neurodevelopment, brain maturation, and aging will inform mapping of brain-related GWAS and will be crucial to improving precision medicine.

Notable technical limitations reduce the broad generalizability of our GxE analyses. First, reflecting the present state of GWAS, the variants tested were identified in exclusively European-

ancestry data and excluded the MHC locus. Moreover, even some of the most recent publicly available GWAS remain underpowered, overall biasing the MPRA library towards specific disorders (e.g., Eating Disorders, PTSD and OCD had very few variants included). Given this bias, our finding that IL-6-responsive ABC genes were uniquely enriched for PTSD despite the low proportion of tested variants is particularly surprising (**Figure 6B**). Second, our library design prioritized brain eQTL from the adult DLPFC, whereas enhancer activity was quantified in hiPSC-neurons that more resemble fetal-like glutamatergic neurons. That our results showed higher concordance with fetal brain, and a lack of concordance to adult DLPFC (**Figure 2**), suggests that the degree or direction of eGene regulation may be altered by age and environment, in line with previous literature[94,95,97]. Third, this may be the first neuronal MPRA conducted in multiple donors; while enhancer activity was highly correlated between donors at baseline (**SI Figure 6**), inter-donor variability in cue-specific transcriptional activity was less so, particularly for IFNa-2b response. We caution that donor genotype and polygenic context may influence functional genomics[100,101]. Fourth, as MPRA-validated regulatory elements were tested independent from their endogenous context, there was an inherent loss of information regarding chromatin accessibility at the endogenous location[102]. Here, we address this through the integration of matched cue-specific ATAC-sequencing, RNA-sequencing, and TF binding affinities to predict cell-type and cue-specific gene targets of enhancer activity[72,73]. These models require additional validation through cue and cell-type specific crisprQTL[103] or prime-editing. Fifth, technical limitations in MPRAs restricted tested CREs to relatively short DNA fragments flanking prioritized variants, potentially omitting crucial portions of larger regulatory regions, a limitation addressed by recent MPRA adaptations (e.g., tiling MPRAs and technical advances in oligo synthesis for library design)[79,91,92]. Finally, drug repurposing databases need to expanded across dose ranges, exposure times, drugs, and cell-types[76,104,105] to improve reproducibility (i.e., concordance between cMAP releases 1 and 2 is low[105], and both cMAP releases were similarly discordant with a third drug compendium[105]). Future studies of cue-specific GxE effects across larger libraries of variants, additional cell-types[9,12,35] (particularly brain-specific immune cells), contexts, doses, and timepoints, and ultimately within more physiologically relevant brain organoids[10,106,107] via emerging single cell MPRA methods[108], and across an expanded number of donors via village-in-a-dish[109–111], will be crucial for further dissection of how immune activation during fetal development contributes to brain disorder risk.

With broad relevance across complex traits and diseases, we demonstrated that it is critical to experimentally resolve dynamic genetic regulation across exposures in a neuronal context. Downstream target genes of cue-specific CREs were uniquely enriched for complex brain disorders and common comorbid metabolic and immune syndromes. FDA-approved medications were predicted to reverse many GxE regulatory interactions, representing potential novel therapeutic interventions for high-risk individuals immediately following environmental exposures, some of which are already established as safe to take during pregnancy[112,113]. Thus, the clinical impact of resolving GxE interactions include preventative measures (improved maternal care, public policy to alleviate life stress, early life intervention for high-risk individuals) and care of current patients (drug repurposing, patient stratification by immune status, personalized prescription). For example, cognitive impairment in SCZ has been linked to increased inflammatory cytokines and to imbalances in cortisol[114]. We identified hundreds of GWAS variants that confer greater susceptibility to complex brain disorders following developmental exposure to stress and inflammation, mapped risk-associated genes, and predicted novel points of therapeutic intervention, altogether informing the influence of GxE interactions on mental health outcomes.

Methods

Selection of predicted cis-expression quantitative trait loci (cis-eQTLs):

Variants selected for inclusion in the MPRA library were prioritized from nine GWAS (AD, ADHD, AN, ASD, BIP, MDD, PTSD, SCZ, and NEU) using Bayesian co-localization (coloc2[58,59]) and transcriptomic imputation (S-PrediXcan[60,61]) (**SI Figure 1**). For the former, overlapping significant GWAS loci and Dorsolateral Pre-frontal Cortex (DLPFC)[8] eQTLs from the Common Mind Consortium (CMC) were tested for co-localization using coloc2[59]. The most probable causal eQTLs from colocalized loci (PPH4>=0.5) were selected, along with all SNPs in high LD (r^2 >= 0.9). For the latter, all SNPs within the predictor models of Bonferroni-corrected significant trait-associated CMC DLPFC S-PrediXcan genes (p<~$4.64x10^{-6}$ (0.05/10786)) and all SNPs in high LD (r^2 >= 0.9) with them were selected.

50 positive and 50 negative controls were selected from SNPs (i) producing the 50 greatest and 50 least transcriptional shifts based on a previous SCZ and AD MPRA[115] and (ii) present in the CMC DLPFC dataset. Additional negative controls were selected from significant BIP GWAS loci that (i) did not colocalize (PPH4 < 0.1) and (ii) were not significant CMC DLPFC eQTLs. While our methods for identification were expression-based and greatly differed from the MPRA used to select the controls, four positive controls were also identified by our methods, most notably rs4702 the top causal SNPs for *FURIN* expression. After accounting for SNPs identified through multiple strategies, and removal of SNPs with sequences containing restriction digest sites, we synthesized a library of ~4,500 SNPs (~10,000 variants) will Oligonucleotides were synthesized by Agilent and cloned into the lentiMPRA vector[81]. We performed a power analysis to determine size limitations of our MPRA; with 10000 SNPs, 50 barcodes per SNP, activity standard deviation of 1 (typical range = 0.3-2), and 3 biological replicates, the power of a t-test to detect differential variant shifts of 0.75 or greater (≥ 5 times as much mRNA per input DNA) at a Bonferroni corrected alpha=0.05 level is 100%[10].

Lenti-MPRA library preparation and viral titration: The MPRA library was generated according to published lenti-MPRA protocols with slight modifications[31]. Briefly, 200 base pair oligonucleotides flanking each prioritized SNP were synthesized by Agilent to create an MPRA library of ~9,500 neuropsychiatric associated variants. The Agilent oligo pool was PCR amplified and a minimal promoter and spacer sequence added downstream of the CRE. Amplified fragments were purified and amplified again for 15 cycles to add a random 15bp sequence to serve as a unique barcode. Barcoded fragments were inserted in the *Sbf*I/*Age*I site of the pLS-SceI vector (AddGene #13772) and then transformed into 10-beta competent cells (NEB, C3020) via electroporation. Bacterial colonies were grown overnight on Ampicillin-positive plates and midi-prepped for plasmid collection. The quality of the purified plasmid was evaluated by Sanger Sequencing of 16 colonies at random. CRE-barcode associations were identified by sequencing of the purified plasmid (MiSeq; paired-end; 15milion reads). 2nd-generation lentiviral packaging of the purified plasmid was performed by the viral core at Boston's Children Hospital. To determine MOI and approximation of appropriate viral volume we infected day 14 iGLUTs (0, 1, 2, 4, 8, 10, 16, 32, 64 µL) with control lentivirus (pLS-SV40-mP-EGFP; AddGene #137724) and harvested for 48hrs later. Following DNA isolation, we performed qPCR to calculate the MOI based the relative ratios of genomic DNA to inserted viral DNA (after subtracting background noise caused by residual backbone DNA).

NGN2-glutamatergic neuron induction of clonalized hiPSC lines[32,33]. Clonal hiPSCs from two neurotypical donors of European ancestry with average schizophrenia PRS and no history of psychiatric diagnoses (#3182 (XX) and #2607 (XY)) were generated by lentiviral transduction with pLV-TetO-hNGN2-eGFP-Neo and lentiviral FUW-M2rtTA (Addgene #20342), followed by antibiotic selection and clonal expansion. Stably selected clones were validated to ensure robust cell survival, expression of fluorescent tags, and transgene expression. hiPSCs were maintained in StemFlex™ Medium (ThermoFisher #A3349401) and passaged with EDTA (Life Technologies #15575-020).

On day 1, medium was switched to non-viral induction medium (DMEM/F12 (Thermofisher, #10565018), 1% N-2 (Thermofisher, #17502048), 2% B-27-RA (Thermofisher, #12587010)) and doxycycline (dox) was added to each well at a final concentration of 1 µg/mL. At day 2, transduced hiPSCs were treated with 500 µg/mL G418 (Thermofisher, #10131035). At day 4, medium was replaced including 1 µg/mL dox and 4 µM cytosine arabinoside (Ara-C) to reduce the proliferation of non-neuronal cells. On day 5, young neurons were dissociated with Accutase Cell Detachment Solution (Innovative Cell Technologies, # AT-104), counted and seeded at a density of $1x10^6$ per well of a Matrigel-coated 12-well plate. Medium was switched to Brainphys neuron medium (Brainphys (STEMCELL, # 05790), 1% N-2, 2% B27-RA, 1 µg/mL Natural Mouse Laminin (Thermofisher, # 23017015), 10 ng/mL BDNF (R&D, #248), 10 ng/mL GDNF (R&D, #212), 500 µg/mL Dibutyryl cyclic-AMP (Sigma, #D0627), 200 nM L-ascorbic acid (Sigma, # A4403)). For seeding, 10 µM Thiazovivin (Millipore, #S1459), 500 µg/mL G418 and 4 µM Ara-C and 1 µg/mLdox were added. At day 6, medium was replaced with Brainphys neuron medium with 4 µM Ara-C and 1 µg/mL dox. Subsequently, 50% of the medium was replaced with fresh neuronal medium (lacking dox and Ara-C) once every other day until the neurons were harvested at d21.

Lentiviral infections of iGLUTs and DNA/RNA barcode sequencing. Day 21 iGLUTs were spinfected (1krcf for 1 hr @37C, slow accel, slow deceleration) with lenti-MPRA library, (based on titrations of the control virus from the Gordon et al. 2020 lentiMPRA Nature Protocol Supplement). 24 hours after spinfections, full media was replaced to remove un-integrated virus. At 48 hours post-infection, cells were treated with context cues or basal media. The number of cells required pre-replicate was calculated according to the Gordon et al. 2020 protocol. On average, 6mil cells were seeded per replicate. 72hrs post-lentiviral-infection, and 48 hrs post-exposure to stress or inflammatory compounds neuronal cells were washed three times and harvested using AllPrep DNA/RNA mini kit (Qiagen) and the libraries prepped as previously described. The libraries were sequenced as paired end reads on a NextSeq 2x50 on S2 flow cell (3.3-4.1 B reads/cell) by the New York Genome Center.

Compound	Solvent	Supplier	Product #	Conc.
Human-recombinant IL-6	UltraPure H2O	Sigma/Aldrich	GF338	60 ng/mL
Human-recombinant INFa2-b	UltraPure H2O	Mount Sinai Pharmacy	NDC 0085-4350-01	500 IU/mL
Hydrocortisone	*17.1 µM EtOH*	Sigma/Aldrich	H0888	1000nM

Phenotyping

NGN2-glutamatergic neuron induction of hiPSC-derived NPCs for phenotypic assays[32,33]. hiPSCs-derived NPCs were dissociated with Accutase Cell Detachment Solution (Innovative Cell Technologies, #AT-104), counted and transduced with rtTA (Addgene 20342) and *NGN2* (Addgene 99378) lentiviruses in StemFlex media containing 10 µM Thiazovivin (Millipore, #S1459). They were subsequently seeded at $1x10^6$ cells/well in the prepared 6-well plate. On day 1, medium was switched to non-viral induction medium (DMEM/F12 (Thermofisher, #10565018), 1% N-2 (Thermofisher, #17502048), 2% B-27-RA (Thermofisher, #12587010)) and doxycycline (dox) was added to each well at a final concentration of 1 µg/mL. At day 2, transduced hiPSCs were treated with 500 µg/mL G418 (Thermofisher, #10131035). At day 4, medium was replaced including 1 µg/mL dox and 4 µM cytosine arabinoside (Ara-C) to reduce the proliferation of non-neuronal cells. On day 5, young neurons were dissociated with Accutase Cell Detachment Solution (Innovative Cell Technologies, #AT-104), counted and seeded at a density of $1x10^6$ per well of a Matrigel-coated 12-well plate. Medium was switched to Brainphys neuron medium (Brainphys (STEMCELL, # 05790), 1% N-2, 2% B27-RA, 1 µg/mL Natural Mouse Laminin

(Thermofisher, # 23017015), 10 ng/mL BDNF (R&D, #248), 10 ng/mL GDNF (R&D, #212), 500 µg/mL Dibutyryl cyclic-AMP (Sigma, #D0627), 200 nM L-ascorbic acid (Sigma, # A4403)). For seeding, 10 µM Thiazovivin (Millipore, #S1459), 500 µg/mL G418 and 4 µM Ara-C and 1 µg/mLdox were added. At day 6, medium was replaced with Brainphys neuron medium with 4 µM Ara-C and 1 µg/mL dox. Subsequently, 50% of the medium was replaced with fresh neuronal medium (lacking dox and Ara-C) once every other day until the neurons were harvested at d21.

Neurite analysis: Day 7 iGLUTs were seeded as $1.5x10^4$ cells/well in a 96-well plate coated with 4x Matrigel at day 3 followed by half medium changes until the neurons were fixed at day 7. At day 5, cells were treated for 48hrs with either hCort (1000nM), IL-6 (60 ng/µL), INFa-2b (500 UI/mL), or matched vehicles. Following cue exposure, cultures were fixed using 4% formaldehyde/sucrose in PBS with Ca^{2+} and Mg^{2+} for 10 minutes at room temperature (RT). Fixed cultures were washed twice in PBS and permeabilized and blocked using 0.1% Triton/2% Normal Donkey Serum (NDS) in PBS for two hours. Cultures were then incubated with primary antibody solution (1:1000 MAP2 anti chicken (Abcam, ab5392) in PBS with 2% NDS) overnight at 4°C. Cultures were then washed 3x with PBS and incubated with secondary antibody solution (1:500 donkey anti chicken Alexa 647 (Life technologies, A10042) in PBS with 2% NDS) for 1 hour at RT. Cultures were washed a further 3x with PBS with the second wash containing 1 µg/ml DAPI. Fixed cultures were then imaged on a CellInsight CX7 HCS Platform with a 20x objective (0.4 NA) and neurite tracing analysis performed using the neurite tracing module in the Thermo Scientific HCS Studio 4.0 Cell Analysis Software. 12 wells were imaged per condition across a minimum 2 independent cell lines, with 9 images acquired per well for neurite tracing analysis. A one-way ANOVA with a post hoc Bonferroni multiple comparisons test was performed on data for neurite length per neuron using Graphpad Prism.

Synapse analyses: Commercially available primary human astrocytes (pHAs, Sciencell, #1800; isolated from fetal female brain) were seeded on D3 at $1.7x10^4$ cells per well on a 4x Matrigel-coated 96 W plate in neuronal media supplemented with 2% fetal bovine serum (FBS). iGLUTs were seeded over the astrocyte monolayer as $1.5x10^5$ cells/well at day 5 post induction. Half changes of neuronal media were performed twice a week until fixation. At day 13, iGLUTs were treated with 200 nM Ara-C to reduce the proliferation of non-neuronal cells in the culture. At day 18, Ara-C was completely withdrawn by full medium change followed by half medium changes until the neurons were fixed at day 21. At day 21, cells were treated for 48hrs with hCort (1000nM), IL-6 (60 ng/µL), IFNa-2b (500 IU/mL), or matched vehicles. Following exposure, cultures were fixed and immune-stained as described previously, with an additional antibody stain for Synapsin1 (primary antibody: 1:500 Synapsin1 anti mouse (Synaptic Systems, 106 011); secondary antibody: donkey anti mouse Alexa 568 (Life technologies A10037)). Stained cultures were imaged and analyzed as above using the synaptogenesis module in the Thermo Scientific HCS Studio 4.0 Cell Analysis Software to determine SYN1+ puncta number, area, and intensity per neurite length in each image. 20 wells were imaged per condition across a minimum of 2 independent cell lines, with 9 images acquired per well for synaptic puncta analysis. A one-way ANOVA with a post hoc Bonferroni multiple comparisons test was performed on data for puncta number per neurite length using Graphpad Prism.

Antibody	Species	Supplier	Product #	Dilution
MAP2	Ck	Abcam	ab5392	1:500
SYNAPSIN1	Ms	Synaptic Systems	106 011	1:500
Alexa 568 anti-Mouse	Ms	Life technologies	A10037	1:500
Alexa 647 anti-Chicken	Ck	Life technologies	A10042	1:500

Multiple Electrode array (MEA): Commercially available primary human astrocytes (pHAs, Sciencell, #1800; isolated from fetal female brain) were seeded on D3 at $1.7x10^4$ cells per well on a 4x Matrigel-coated 48 W MEA plate (catalog no. M768-tMEA-48W; Axion Biosystems) in neuronal media supplemented with 2% fetal bovine serum (FBS). At D5, iGLUTs were detached, spun down and seeded on the pHA cultures at $1.5x10^5$ cells per well. Half changes of neuronal media supplemented with 2% FBS were performed twice a week until day 42. At day 13, co-cultures were treated with 200 nM Ara-C to reduce the proliferation of non-neuronal cells in the culture. At Day 18, Ara-C was completely withdrawn by full medium change. At day 26, cells were treated for 48hrs with hCort (1000nM), IL-6 (60 µg/mL), IFNa-2b (500 IU/mL), or matched vehicles. Following exposure, electrical activity of iGLUTs was recorded at 37°C using the Axion Maestro MEA reader (Axion Biosystems). Recording was performed via AxiS 2.4. Batch mode/statistic compiler tool was run following the final recording. Quantitative analysis of the recording was exported as Microsoft excel sheet. Data from 6-12 biological replicates were analyzed using GraphPad PRISM 6 software or R.

Context-cue Specific RNAseq: RNA Sequencing libraries were prepared using the Kapa Total RNA library prep kit. Paired-end sequencing reads (100bp) were generated on a NovaSeq platform. Raw reads were aligned to hg19 using STAR aligner[100] (v2.5.2a) and gene-level expression were quantified by featureCounts[101] (v1.6.3) based on Ensemble GRCh37.70 annotation model. Genes with over 10 counts per million (CPM) in at least four samples were retained. After filtering, the raw read counts were normalized by the voom[102] function in limma and differential expression was computed by the moderated t-test implemented in limma[103]. Differential gene expression analysis was performed between each cue and paired vehicle. Bayes shrinkage (limma::eBayes) estimated modified t- and p- values and identified differentially expressed genes (DEGs) based on an FDR <= 0.05 (limma::TopTable)[104]. GO/pathways were evaluated using Gene-set Enrichment Analysis (GSEA)[105]. In these analyses, the t-test statistics from the differential expression contrast were used to rank genes in the GSEA using the R package ClusterProfiler[106]. Permutations (up to 100,000 times) were used to assess the GSEA enrichment P value.

Meta-analysis of gene expression across contexts. We performed a meta-analysis and Cochran's heterogeneity Q-test (METAL[40]) using the p-values and direction of effects (t-statistic), weighted according to sample size across all sets of perturbations (Target vs. Scramble DEGs). Genes were defined as convergent if they (1) had the same direction of effect across cue exposure (2) were Bonferroni significant in our meta-analysis (Bonferroni adjusted p-value <= 0.05), and (3) had a heterogeneity p-value = >0.05 (**SI Figure 1D**).

Context-cue Specific ATAC-Seq: Mature neurons were washed with 500uL of PBS (-Ca/-Mg)-0.5mM EDTA per well of a 12-well plate. Then, 300uL dissociation solution (0.042 U/µL papain suspension (Worthington-Biochem LS003126) in HBSS (Thermofisher #14025076)-10mM HEPES (Thermofisher #J61275AE)-0.5mM EDTA (Life Technologies #15575-020), pre-activated at 37C for 5 minutes) supplemented with 0.017U/µL DNase (Thermofisher #EN0521) and 1x Chroman I was added to each well before incubating the plate at 37C for 10 minutes, shaking at 125rpm. 600uL deactivating solution (DMEM-FBS-Chroman I) was then added to each well, and cells were dissociated into single cells by pipetting gently. For each condition, cells from 4 wells of a 12-well-plate were combined into a single 15mL conical tube for higher yield. After spinning at 600g for 5 minutes at room temperature, cells were resuspended in 310uL of DMEM (Thermofisher #10566-016)-10% FBS. Then, the cell suspension was filtered through a 37um reversible strainer and frozen in DMEM-10% FBS-10% DMSO.

ATAC sequencing library prep and sequencing were performed by the Yale Sequencing Core. The adaptor sequence for pair-end sequencing was removed using trim_galore[116] and sequencing quality measure by FastQC[117] and MutliQC[118]. Data was aligned with Bowtie2[119]

against hg38 reference genome including rare SNVs. Mitochondrial reads were removed, sam files sorted and indexed, and converted to compressed BAM files with samtools[120] and ATAC peaks called using Genrich[121]. Differential peak activity analysis was performed with edgeR[122,123] and csaw[124].

Processing of MPRA sequencing data. Barcode-CRE association was performed as previously described using the association utility of MPRAflow v2.3.5[31] (run as:). We demultiplexed the indexed DNA and RNA libraries and generated fastq files with bcl2fastq v2.20 and used the count utility of MPRAflow 2.3.5 with the --mpranalyze flag included (run as: nextflow run count.nf -w –experiment-file –dir –outdir –labels –design –bc-length 14 –umi-length 16) to compute the activity score for each element and produce count files formatted for analysis with MPRAnalyze[125]. We filtered variants using a minimum threshold of 10 observed barcodes per variant and used a generalized linear model to quantify CRE with significantly greater transcriptional activity compared to scramble controls using MPRAnalyze::analyzeQuantification and MPRAAnalyze::testEmpirical functions. We performed comparative analysis on the normalized counts to identify differences in transcriptional activity between cue exposures and vehicle using MPRAnalyze::analyzeComaprative and MPRAnalyze::LRT function. Variants with an FDR adjusted p-value<=0.1 were considered significantly differentially active.

Comparison of regulatory activity across replicates, donors, and cue exposures. Transcriptional activity, measured as the normalized log2 DNA and RNA counts per CRE, across conditions is strongly correlated between replicates (Pearson's rho-correlation 0.98-1.00; **SI Figure 4**) and the log2 normalized RNA/DNA ratios are strongly correlated between donors (rho=0.50-0.71) (**SI Figure 5a**). Across conditions 3,440-3747 of CRE were captured (minimum requirement of 10 barcodes each) and the number of barcodes per unique CRE were highly correlated between CRE shared across all conditions (rho 0.968-0.999; nCRE=3139). There was no significant difference in mean number of barcodes per insert or the proportion of CRE by prioritization method or disorder association across the conditions (**SI Figure 5b-e**).

Analysis of allelic shifts in MPRA activity and comparison to eQTL datasets. For CRE where both the alternative and reference allele were captured with a minimum of 10 barcodes, we tested for significant shifts in transcriptional activity.-To calculate significant allelic shifts in activity, we tested each allelic pair in a generalized linear model (log2(RNA) ~ log2(DNA) + replicate + barcode + n_bc) as in the saturation mutagenesis analysis from MPRAflow[31]. Variant differences with an FDR adjusted p-value<=0.05 were considered significantly differentially active. We then tested the correlation between MPRA allelic shifts and post-mortem single cell[16], fetal brain[65], and the CMC adult DLPFC eQTL betas[96] (filtering for significant MPRA activity but including non-significant eQTLs) using a generalized linear model [Abs(MPRA allelic shift) ~ abs(eQTL Beta) + log_Dis_TSS + Gene + CellType]. Linear correlation coefficients with an FDR adjusted p-value of <= 0.05 were considered significant, and coefficients with unadjusted p-values <=0.05 were considered nominally significant.

Functional enrichment of significantly active MPRA variants. Functional enrichment WebGestalt (WEB-based Gene SeT AnaLysis Toolkit)[82]. Over-representation analysis (ORA) was performed on all significantly active variants at baseline and after cue-exposures and all significantly differentially active variants for each cue compared to baseline against a list of common variant target genes pulled from PGC-GWAS summary statistics using MAGMA[74].

Overlap of active CRE with cCRE ENCODE annotations. We assessed overlap of active CRE in these MPRA with previously annotated enhancer-like sequences across the human genome (hg38) from the cCRE Encode Registry[81,82]. To further explore the relationship between CTCF binding and condition-specific transcriptional activity, we scanned each 200bp CRE sequence to identify and score best matches of six highly conserved core CTCF binding motifs (CTCFBSDB

2.0)[126,127]. We assessed the impact of CTCF binding affinities across these motifs on transcriptional activity using a generalized linear model (MPRA median z-score ~ motif binding score + orientation + variant + binding motif distance from SNP). Linear correlation estimates with an FDR adjusted p-value <0.05 were considered significant.

TF motif enrichment analysis We performed TF binding enrichment across all significantly active CRE for each condition using the MEME Suite Simple Enrichment Analysis (SEA)[128] with the Human HOCOMOCO V11 reference. We performed a differential enrichment analysis comparing motif binding in significant CRE following exposure to hCort, IL-6, and INFα with Baseline by setting the control sequences as those significant at baseline. Results were filtered based on expression data of in DIV24 iGLUTs described above.

DeltaSVM and allele-specific binding affinity scoring with MotifBreaker. We calculated a deltaSVM score[69,70] which represent predicted changes in transcriptional activity due to changes in TF binding affinity, across all sequence tested in the MPRA using high-confidence 94 high-confidence SVM models created in from HI-SELEX experiment testing 270 human TFs and 95,886 noncoding variants in the human genome[69,70]. Of these 94 TFs, 74 are expressed in iGLUTs and used for downstream analyses. To identify allelic effects on TF binding for CRE that were specifically differentially active after an exposure compared to baseline, we used the motifbreakR package[68] and filtered for strong allelic effects of TFs expressed in DIV24 iGLUTs.

Activity-by-Contact prediction of context-specific regulatory element target genes. To predict target genes of condition-specific enhancer activity, we scored enhancer-gene interaction using STARE[73]. STARE combines an adapted Activity-By-Contact (ABC)[72] interaction modeling with TF binding affinities in regions to summarize these affinities at the gene level. For each condition, we used the median z-score of each CRE tested in the MPRA to represent “Activity”, and the condition-specific ATAC-sequencing peaks to represent “Contact” in the model.

Over-representation analysis and biological theme comparison of ABC genes. To identify pathway enrichments unique to context-specific regulatory activity, we performed biological theme comparison using ClusterProfiler[129]. And gene set enrichment for GWAS catalogue risk genes using the GENE2FUNC query tool of FUMA GWAS[75].

Drug prioritization based on perturbation signature reversal in LiNCs Neuronal Cell Lines: To identify drugs that could reverse cue-specific GReX predicted by the ABC model, we used the Query tool from The Broad Institute’s Connectivity Map (Cmap) Server[76]. Briefly, the tool computes weighted enrichment scores (WTCS) between the query set and each signature in the Cmap LINCs gene expression data (dose, time, drug, cell-line), normalizes the WRCS by dividing by signed mean w/in each perturbation (NCS), and computes FDR as fraction of “null signatures” (DMSO) where the absolute NCS exceeds reference signature[127]. We prioritized drugs that reversed signatures specifically in neuronal cells (either neurons (NEU) of neural progenitor cells (NPCs) with NCS <= -1.00, FDR<=0.05) and filtered for drugs that are currently launched or in clinical trial according to the Broad Institute Repurposing Data Portal.

STATEMENT OF ETHICS

Ethical approval was not required because the hiPSC lines, lacking association with any identifying information and widely accessible from a public repository, are thus not considered to be human subjects research. Post-mortem DLPFC data are similarly lacking identifiable information and are not considered human subjects research.

CONFLICT OF INTEREST STATEMENT

K.J.B is a scientific advisor to Rumi Scientific Inc. and Neuro Pharmaka Inc. All other authors declare no conflicts of interest

FUNDING SOURCES

This work was supported by F31MH130122 (K.G.R), R01MH109897 (K.J.B.), R56MH101454 (K.J.B., L.H.), R01MH123155 (K.J.B.) and R01ES033630 (L.H., K.J.B.), R01MH124839 (LMH), R01MH106056 (K.J.B) U01DA047880 (K.J.B), R01DA048279 (K.J.B), DOD TP220451 (K.J.B., L.H.), and by the State of Connecticut, Department of Mental Health and Addiction Services. This publication does not express the views of the Department of Mental Health and Addiction Services or the State of Connecticut.

AUTHOR CONTRIBUTIONS

The paper was written by K.G.R., L.H. and K.J.B., with input from all authors. All high-throughput sequencing data and downstream analyses were performed by K.G.R.; L.D. provided code and guidance in conducting Bayesian colocalization analyses. S.L and M.J performed cue-specific ATAC experiments. P.M.D performed dose-dependent morphological assays and analysis. M.F.G and K.G.R. performed cell-line clonalization. K.G.R performed MPRA library preparation and MPRA experiments with the assistance of M.F.G, S.C, S.C, and A.S.

DATA AND CODE AVAILABILITY

All source donor hiPSCs have been deposited at the Rutgers University Cell and DNA Repository (study 160; http://www.nimhstemcells.org/).

Full sequencing data, processed data, and accompanying code reported in this paper will be made available through GEO and Synapse upon publication.

REFERENCES

1. Edwards, S. L., Beesley, J., French, J. D. & Dunning, M. Beyond GWASs: Illuminating the dark road from association to function. *American Journal of Human Genetics* vol. 93 779–797 Preprint at https://doi.org/10.1016/j.ajhg.2013.10.012 (2013).

2. Maeda, R. K. & Karch, F. Gene expression in time and space: Additive vs hierarchical organization of cis-regulatory regions. *Current Opinion in Genetics and Development* **21**, 187–193 (2011).

3. Young, H., Cote, A. & Huckins, L. M. Chapter 14 - Integration with systems biology approaches and -omics data to characterize risk variation. in *Psychiatric Genomics* (eds.

Tsermpini, E. E., Alda, M. & Patrinos, G. P.) 289–315 (Academic Press, 2022). doi:10.1016/B978-0-12-819602-1.00017-6.

4. Bellavance, M.-A. & Rivest, S. The HPA – Immune Axis and the Immunomodulatory Actions of Glucocorticoids in the Brain. *Front. Immunol.* **5**, (2014).
5. SILVERMAN, M. N., PEARCE, B. D., BIRON, C. A. & MILLER, A. H. Immune Modulation of the Hypothalamic-Pituitary-Adrenal (HPA) Axis during Viral Infection. *Viral Immunol* **18**, 41–78 (2005).
6. Barabási, B. *et al.* Role of interleukin-6 and interleukin-10 in morphological and functional changes of the blood–brain barrier in hypertriglyceridemia. *Fluids and Barriers of the CNS* **20**, 15 (2023).
7. Fioravanti, J. *et al.* The Fusion Protein of IFN-α and Apolipoprotein A-I Crosses the Blood–Brain Barrier by a Saturable Transport Mechanism. *The Journal of Immunology* **188**, 3988–3992 (2012).
8. Wu, W. L., Hsiao, E. Y., Yan, Z., Mazmanian, S. K. & Patterson, P. H. The placental interleukin-6 signaling controls fetal brain development and behavior. *Brain, Behavior, and Immunity* **62**, 11–23 (2017).
9. Sarieva, K. *et al.* Pluripotent stem cell-derived neural progenitor cells can be used to model effects of IL-6 on human neurodevelopment. *Dis Model Mech* **16**, dmm050306 (2023).
10. Sarieva, K. *et al.* Human brain organoid model of maternal immune activation identifies radial glia cells as selectively vulnerable. *Mol Psychiatry* 1–13 (2023) doi:10.1038/s41380-023-01997-1.
11. Zheng, L.-S. *et al.* Mechanisms for Interferon-α-Induced Depression and Neural Stem Cell Dysfunction. *Stem Cell Reports* **3**, 73–84 (2014).
12. Seah, C. *et al.* Modeling gene × environment interactions in PTSD using human neurons reveals diagnosis-specific glucocorticoid-induced gene expression. *Nat Neurosci* **25**, 1434–1445 (2022).

718 13. Lonsdale, J. *et al.* The Genotype-Tissue Expression (GTEx) project. *Nature Genetics* **45**,
719 580–585 (2013).
720 14. Aguet, F. *et al.* Genetic effects on gene expression across human tissues. *Nature* **550**, 204–
721 213 (2017).
722 15. The GTEx Consortium atlas of genetic regulatory effects across human tissues. *Science*
723 **369**, 1318–1330 (2020).
724 16. Bryois, J. *et al.* Cell-type-specific cis-eQTLs in eight human brain cell types identify novel
725 risk genes for psychiatric and neurological disorders. *Nat Neurosci* **25**, 1104–1112 (2022).
726 17. Donovan, M. K. R., D'Antonio-Chronowska, A., D'Antonio, M. & Frazer, K. A. Cellular
727 deconvolution of GTEx tissues powers discovery of disease and cell-type associated
728 regulatory variants. *Nature Communications* **11**, 955 (2020).
729 18. Aygün, N. *et al.* Inferring cell-type-specific causal gene regulatory networks during human
730 neurogenesis. *Genome Biology* **24**, 130 (2023).
731 19. Dimas, A. S. *et al.* Sex-biased genetic effects on gene regulation in humans. *Genome*
732 *Research* **22**, 2368–2375 (2012).
733 20. Moore, S. R. *et al.* Sex differences in the genetic regulation of the blood transcriptome
734 response to glucocorticoid receptor activation. *Transl Psychiatry* **11**, 1–14 (2021).
735 21. Oliva, M. *et al.* The impact of sex on gene expression across human tissues. *Science* **369**,
736 eaba3066 (2020).
737 22. Alasoo, K. *et al.* Shared genetic effects on chromatin and gene expression indicate a role for
738 enhancer priming in immune response. *Nat Genet* **50**, 424–431 (2018).
739 23. Davenport, E. E. *et al.* Discovering in vivo cytokine-eQTL interactions from a lupus clinical
740 trial. *Genome Biology* **19**, 168 (2018).
741 24. Maranville, J. C. *et al.* Interactions between Glucocorticoid Treatment and Cis-Regulatory
742 Polymorphisms Contribute to Cellular Response Phenotypes. *PLoS Genet* **7**, e1002162
743 (2011).

744 25. Arloth, J. *et al.* Genetic Differences in the Immediate Transcriptome Response to Stress
745 Predict Risk-Related Brain Function and Psychiatric Disorders. *Neuron* **86**, 1189–1202
746 (2015).
747 26. Arloth, J. *et al.* DeepWAS: Multivariate genotype-phenotype associations by directly
748 integrating regulatory information using deep learning. *PLOS Computational Biology* **16**,
749 e1007616 (2020).
750 27. Yazar, S. *et al.* Single-cell eQTL mapping identifies cell type–specific genetic control of
751 autoimmune disease. *Science* **376**, eabf3041 (2022).
752 28. Yamaguchi, K. *et al.* Splicing QTL analysis focusing on coding sequences reveals
753 mechanisms for disease susceptibility loci. *Nat Commun* **13**, 4659 (2022).
754 29. Inoue, F. *et al.* A systematic comparison reveals substantial differences in chromosomal
755 versus episomal encoding of enhancer activity. *Genome Research* **27**, 38–52 (2017).
756 30. Inoue, F., Kreimer, A., Ashuach, T., Ahituv, N. & Yosef, N. Identification and Massively
757 Parallel Characterization of Regulatory Elements Driving Neural Induction. *Cell Stem Cell*
758 **25**, 713-727.e10 (2019).
759 31. Gordon, M. G. *et al.* lentiMPRA and MPRAflow for high-throughput functional
760 characterization of gene regulatory elements. *Nature Protocols* **15**, 2387–2412 (2020).
761 32. Mulvey, B., Lagunas, T. & Dougherty, J. D. Massively Parallel Reporter Assays: Defining
762 Functional Psychiatric Genetic Variants across Biological Contexts. *Biological Psychiatry* **0**,
763 (2020).
764 33. Mulvey, B., Selmanovic, D. & Dougherty, J. D. Sex Significantly Impacts the Function of
765 Major Depression–Linked Variants In Vivo. *Biological Psychiatry* **94**, 466–478 (2023).
766 34. Mulvey, B. & Dougherty, J. D. Transcriptional-Regulatory Convergence Across Functional
767 MDD Risk Variants Identified by Massively Parallel Reporter Assays. 2021.03.05.434177
768 Preprint at https://doi.org/10.1101/2021.03.05.434177 (2021).

769 35. Rummel, C. K. *et al.* Massively parallel functional dissection of schizophrenia-associated
770 noncoding genetic variants. *Cell* **186**, 5165-5182.e33 (2023).
771 36. Kreimer, A. *et al.* Massively parallel reporter perturbation assays uncover temporal
772 regulatory architecture during neural differentiation. *Nat Commun* **13**, 1504 (2022).
773 37. Daskalakis, N. P., Cohen, H., Cai, G., Buxbaum, J. D. & Yehuda, R. Expression profiling
774 associates blood and brain glucocorticoid receptor signaling with trauma-related individual
775 differences in both sexes. *Proceedings of the National Academy of Sciences of the United*
776 *States of America* **111**, 13529–13534 (2014).
777 38. Smith, S. E. P., Li, J., Garbett, K., Mirnics, K. & Patterson, P. H. Maternal immune activation
778 alters fetal brain development through interleukin-6. *Journal of Neuroscience* **27**, 10695–
779 10702 (2007).
780 39. Armario, A., Hernández, J., Bluethmann, H. & Hidalgo, J. IL-6 deficiency leads to increased
781 emotionality in mice: Evidence in transgenic mice carrying a null mutation for IL-6. *Journal*
782 *of Neuroimmunology* **92**, 160–169 (1998).
783 40. Borovcanin, M. M. *et al.* Interleukin-6 in Schizophrenia-Is There a Therapeutic Relevance?
784 *Front Psychiatry* **8**, 221 (2017).
785 41. Ben-Yehuda, H. *et al.* Maternal Type-I interferon signaling adversely affects the microglia
786 and the behavior of the offspring accompanied by increased sensitivity to stress. *Molecular*
787 *Psychiatry* **25**, 1050–1067 (2020).
788 42. Schaefer, M. *et al.* Prevention of interferon-alpha associated depression in psychiatric risk
789 patients with chronic hepatitis C. *J Hepatol* **42**, 793–798 (2005).
790 43. Baines, K. J. *et al.* Maternal Immune Activation Alters Fetal Brain Development and
791 Enhances Proliferation of Neural Precursor Cells in Rats. *Front Immunol* **11**, 1145 (2020).
792 44. Garbett, K. A., Hsiao, E. Y., Kálmán, S., Patterson, P. H. & Mirnics, K. Effects of maternal
793 immune activation on gene expression patterns in the fetal brain. *Transl Psychiatry* **2**, e98–
794 e98 (2012).

795 45. Laighneach, A., Desbonnet, L., Kelly, J. P., Donohoe, G. & Morris, D. W. Meta-Analysis of
796 Brain Gene Expression Data from Mouse Model Studies of Maternal Immune Activation
797 Using Poly(I:C). *Genes (Basel)* **12**, 1363 (2021).
798 46. Dong, Y. *et al.* Transcriptomic profiling of the developing brain revealed cell-type and brain-
799 region specificity in a mouse model of prenatal stress. *BMC Genomics* **24**, 86 (2023).
800 47. Causal analysis approaches in Ingenuity Pathway Analysis | Bioinformatics | Oxford
801 Academic. https://academic.oup.com/bioinformatics/article/30/4/523/202720.
802 48. Marioni, R. E. *et al.* Correction: GWAS on family history of Alzheimer's disease. *Transl*
803 *Psychiatry* **9**, 161 (2019).
804 49. Demontis, D. *et al.* Discovery of the first genome-wide significant risk loci for attention
805 deficit/hyperactivity disorder. *Nature Genetics* **51**, 63–75 (2019).
806 50. Watson, H. J. *et al.* Genome-wide association study identifies eight risk loci and implicates
807 metabo-psychiatric origins for anorexia nervosa. *Nature Genetics* **51**, 1207–1214 (2019).
808 51. Grove, J. *et al.* Identification of common genetic risk variants for autism spectrum disorder.
809 *Nature Genetics* **51**, 431–444 (2019).
810 52. Mullins, N. *et al.* Genome-wide association study of more than 40,000 bipolar disorder
811 cases provides new insights into the underlying biology. *Nat Genet* **53**, 817–829 (2021).
812 53. Howard, D. M. *et al.* Genome-wide meta-analysis of depression identifies 102 independent
813 variants and highlights the importance of the prefrontal brain regions. *Nature Neuroscience*
814 **22**, 343–352 (2019).
815 54. Arnold, P. D. *et al.* Revealing the complex genetic architecture of obsessive-compulsive
816 disorder using meta-analysis. *Molecular Psychiatry* **23**, 1181–1188 (2018).
817 55. Huckins, L. M. *et al.* Analysis of Genetically Regulated Gene Expression Identifies a
818 Prefrontal PTSD Gene, SNRNP35, Specific to Military Cohorts. (2020)
819 doi:10.1016/j.celrep.2020.107716.

820 56. Trubetskoy, V. *et al.* Mapping genomic loci implicates genes and synaptic biology in
821 schizophrenia. *Nature* **604**, 502–508 (2022).
822 57. Lo, M. T. *et al.* Genome-wide analyses for personality traits identify six genomic loci and
823 show correlations with psychiatric disorders. *Nature Genetics* **49**, 152–156 (2017).
824 58. Pickrell, J. K. *et al.* Detection and interpretation of shared genetic influences on 42 human
825 traits. *Nature Genetics* **48**, 709–717 (2016).
826 59. Giambartolomei, C. *et al.* A Bayesian Framework for Multiple Trait Colocalization from
827 Summary Association Statistics. *A Bayesian framework for multiple trait colocalization from*
828 *summary association statistics* 155481 (2017) doi:10.1101/155481.
829 60. Gamazon, E. R. *et al.* A gene-based association method for mapping traits using reference
830 transcriptome data. *Nature Genetics* **47**, 1091–1098 (2015).
831 61. Barbeira, A. N. *et al.* Exploring the phenotypic consequences of tissue specific gene
832 expression variation inferred from GWAS summary statistics. *Nature Communications* **9**,
833 1–20 (2018).
834 62. Nott, A. *et al.* Brain cell type–specific enhancer–promoter interactome maps and disease-
835 risk association. *Science* **366**, 1134–1139 (2019).
836 63. Agarwal, D. *et al.* A single-cell atlas of the human substantia nigra reveals cell-specific
837 pathways associated with neurological disorders. *Nat Commun* **11**, 1–11 (2020).
838 64. Tewhey, R. *et al.* Direct identification of hundreds of expression-modulating variants using a
839 multiplexed reporter assay. *Cell* **165**, 1519–1529 (2016).
840 65. O'Brien, H. E. *et al.* Expression quantitative trait loci in the developing human brain and their
841 enrichment in neuropsychiatric disorders. *Genome Biol* **19**, 194 (2018).
842 66. Bailey, T. L. & Machanick, P. Inferring direct DNA binding from ChIP-seq. *Nucleic Acids*
843 *Research* **40**, e128 (2012).
844 67. Stelzer, G. *et al.* The GeneCards Suite: From Gene Data Mining to Disease Genome
845 Sequence Analyses. *Current Protocols in Bioinformatics* **54**, 1.30.1-1.30.33 (2016).

68. Coetzee, S. G., Coetzee, G. A. & Hazelett, D. J. motifbreakR: an R/Bioconductor package for predicting variant effects at transcription factor binding sites. *Bioinformatics* **31**, 3847–3849 (2015).

69. Yan, J. *et al.* Systematic analysis of binding of transcription factors to noncoding variants. *Nature* **591**, 147–151 (2021).

70. Yin, Y. *et al.* Impact of cytosine methylation on DNA binding specificities of human transcription factors. *Science* **356**, eaaj2239 (2017).

71. Lee, D. *et al.* A method to predict the impact of regulatory variants from DNA sequence. *Nat Genet* **47**, 955–961 (2015).

72. Fulco, C. P. *et al.* Activity-by-contact model of enhancer–promoter regulation from thousands of CRISPR perturbations. *Nature Genetics* **51**, 1664–1669 (2019).

73. Hecker, D., Behjati Ardakani, F., Karollus, A., Gagneur, J. & Schulz, M. H. The adapted Activity-By-Contact model for enhancer–gene assignment and its application to single-cell data. *Bioinformatics* **39**, btad062 (2023).

74. Leeuw, C. A. de, Mooij, J. M., Heskes, T. & Posthuma, D. MAGMA: Generalized Gene-Set Analysis of GWAS Data. *PLOS Computational Biology* **11**, e1004219 (2015).

75. Watanabe, K., Taskesen, E., van Bochoven, A. & Posthuma, D. Functional mapping and annotation of genetic associations with FUMA. *Nat Commun* **8**, 1826 (2017).

76. Subramanian, A. *et al.* A Next Generation Connectivity Map: L1000 platform and the first 1,000,000 profiles. *Cell* **171**, 1437-1452.e17 (2017).

77. Lin, L.-C. & Sibille, E. Reduced brain somatostatin in mood disorders: a common pathophysiological substrate and drug target? *Front. Pharmacol.* **4**, (2013).

78. Van Derveer, A. B. *et al.* A Role for Somatostatin-Positive Interneurons in Neuro-Oscillatory and Information Processing Deficits in Schizophrenia. *Schizophr Bull* **47**, 1385–1398 (2021).

79. Sommer, I. E. *et al.* Simvastatin Augmentation for Patients With Early-Phase Schizophrenia-Spectrum Disorders: A Double-Blind, Randomized Placebo-Controlled Trial. *Schizophrenia Bulletin* **47**, 1108–1115 (2021).

80. Shen, H. *et al.* Adjunctive therapy with statins in schizophrenia patients: A meta-analysis and implications. *Psychiatry Res* **262**, 84–93 (2018).

81. Kagda, M. S. *et al.* Data navigation on the ENCODE portal. Preprint at http://arxiv.org/abs/2305.00006 (2023).

82. Luo, Y. *et al.* New developments on the Encyclopedia of DNA Elements (ENCODE) data portal. *Nucleic Acids Res* **48**, D882–D889 (2020).

83. Kim, S., Yu, N.-K. & Kaang, B.-K. CTCF as a multifunctional protein in genome regulation and gene expression. *Exp Mol Med* **47**, e166–e166 (2015).

84. Gofin, Y. *et al.* Delineation of a novel neurodevelopmental syndrome associated with PAX5 haploinsufficiency. *Hum Mutat* **43**, 461–470 (2022).

85. Ohtsuka, N. *et al.* GABAergic neurons regulate lateral ventricular development via transcription factor Pax5. *genesis* **51**, 234–245 (2013).

86. MacArthur, J. *et al.* The new NHGRI-EBI Catalog of published genome-wide association studies (GWAS Catalog). *Nucleic Acids Research* **45**, D896–D901 (2017).

87. Cruceanu, C. *et al.* Cell-Type-Specific Impact of Glucocorticoid Receptor Activation on the Developing Brain: A Cerebral Organoid Study. *Am J Psychiatry* **179**, 375–387 (2022).

88. Resztak, J. A. *et al.* Genetic control of the dynamic transcriptional response to immune stimuli and glucocorticoids at single-cell resolution. *Genome Res* **33**, 839–856 (2023).

89. Hall, M. B., Willis, D. E., Rodriguez, E. L. & Schwarz, J. M. Maternal immune activation as an epidemiological risk factor for neurodevelopmental disorders: Considerations of timing, severity, individual differences, and sex in human and rodent studies. *Frontiers in Neuroscience* **17**, (2023).

90. Estes, M. L. & McAllister, A. K. Maternal immune activation: Implications for neuropsychiatric disorders. *Science* **353**, 772–777 (2016).

91. Trifonova, E. A., Mustafin, Z. S., Lashin, S. A. & Kochetov, A. V. Abnormal mTOR Activity in Pediatric Autoimmune Neuropsychiatric and MIA-Associated Autism Spectrum Disorders. *Int J Mol Sci* **23**, 967 (2022).

92. Rosario, F. J. *et al.* Mechanistic Target of Rapamycin Complex 2 Regulation of the Primary Human Trophoblast Cell Transcriptome. *Front Cell Dev Biol* **9**, 670980 (2021).

93. Yao, C. *et al.* Genome-wide mapping of plasma protein QTLs identifies putatively causal genes and pathways for cardiovascular disease. *Nat Commun* **9**, 3268 (2018).

94. Bryois, J. *et al.* Time-dependent genetic effects on gene expression implicate aging processes. *Genome Res.* **27**, 545–552 (2017).

95. Yamamoto, R. *et al.* Tissue-specific impacts of aging and genetics on gene expression patterns in humans. *Nat Commun* **13**, 5803 (2022).

96. Hoffman, G. E. *et al.* CommonMind Consortium provides transcriptomic and epigenomic data for Schizophrenia and Bipolar Disorder. *Sci Data* **6**, 180 (2019).

97. Yao, C. *et al.* Sex- and age-interacting eQTLs in human complex diseases. *Hum Mol Genet* **23**, 1947–1956 (2014).

98. Solmi, M. *et al.* Age at onset of mental disorders worldwide: large-scale meta-analysis of 192 epidemiological studies. *Mol Psychiatry* **27**, 281–295 (2022).

99. Inoue, F., Kreimer, A., Ashuach, T., Ahituv, N. & Yosef, N. Identification and Massively Parallel Characterization of Regulatory Elements Driving Neural Induction. *Cell Stem Cell* **25**, 713-727.e10 (2019).

100. Webber, C. Epistasis in Neuropsychiatric Disorders. *Trends in Genetics* **33**, 256–265 (2017).

101. Andreasen, N. C. *et al.* Statistical Epistasis and Progressive Brain Change in Schizophrenia: An Approach for Examining the Relationships Between Multiple Genes. *Mol Psychiatry* **17**, 1093–1102 (2012).

102. Townsley, K. G., Brennand, K. J. & Huckins, Laura. M. Massively parallel techniques for cataloguing the regulome of the human brain. *Nat Neurosci* **23**, 1509–1521 (2020).

103. Gasperini, M. *et al.* crisprQTL mapping as a genome-wide association framework for cellular genetic screens. 314344 (2018) doi:10.1101/314344.

104. Musa, A., Tripathi, S., Kandhavelu, M., Dehmer, M. & Emmert-Streib, F. Harnessing the biological complexity of Big Data from LINCS gene expression signatures. *PLoS One* **13**, e0201937 (2018).

105. Lim, N. & Pavlidis, P. Evaluation of connectivity map shows limited reproducibility in drug repositioning. *Sci Rep* **11**, 17624 (2021).

106. Benson, C. A. *et al.* Immune Factor, TNFα, Disrupts Human Brain Organoid Development Similar to Schizophrenia—Schizophrenia Increases Developmental Vulnerability to TNFα. *Frontiers in Cellular Neuroscience* **14**, (2020).

107. Swingler, M., Donadoni, M., Bellizzi, A., Cakir, S. & Sariyer, I. K. iPSC-derived three-dimensional brain organoid models and neurotropic viral infections. *J. Neurovirol.* **29**, 121–134 (2023).

108. Zhao, S. *et al.* A single-cell massively parallel reporter assay detects cell-type-specific gene regulation. *Nat Genet* **55**, 346–354 (2023).

109. Neavin, D. R. *et al.* A village in a dish model system for population-scale hiPSC studies. *Nat Commun* **14**, 3240 (2023).

110. Mitchell, J. M. *et al.* Mapping genetic effects on cellular phenotypes with 'cell villages'. *bioRxiv* 2020.06.29.174383 (2020) doi:10.1101/2020.06.29.174383.

111. Wells, M. F. *et al.* Natural variation in gene expression and viral susceptibility revealed by neural progenitor cell villages. *Cell Stem Cell* **30**, 312-332.e13 (2023).

946 112. SMITH, D. D. & COSTANTINE, M. M. The role of statins in the prevention of preeclampsia.
947 *Am J Obstet Gynecol* **226**, S1171–S1181 (2022).
948 113. Meijerink, L. *et al.* Statins in pre-eclampsia or fetal growth restriction: A systematic review
949 and meta-analysis on maternal blood pressure and fetal growth across species. *BJOG: An*
950 *International Journal of Obstetrics & Gynaecology* **130**, 577–585 (2023).
951 114. Martínez, A. L., Brea, J., Rico, S., de los Frailes, M. T. & Loza, M. I. Cognitive Deficit in
952 Schizophrenia: From Etiology to Novel Treatments. *Int J Mol Sci* **22**, 9905 (2021).
953 115. Myint, L. *et al.* Testing the Regulatory Consequences of 1,049 Schizophrenia Associated
954 Variants With a Massively Parallel Reporter Assay. *bioRxiv* 447557 (2018)
955 doi:10.1101/447557.
956 116. GitHub - FelixKrueger/TrimGalore: A wrapper around Cutadapt and FastQC to consistently
957 apply adapter and quality trimming to FastQ files, with extra functionality for RRBS data.
958 https://github.com/FelixKrueger/TrimGalore.
959 117. Babraham Bioinformatics - FastQC A Quality Control tool for High Throughput Sequence
960 Data. https://www.bioinformatics.babraham.ac.uk/projects/fastqc/.
961 118. Ewels, P., Magnusson, M., Lundin, S. & Käller, M. MultiQC: summarize analysis results for
962 multiple tools and samples in a single report. *Bioinformatics* **32**, 3047–3048 (2016).
963 119. Langmead, B. & Salzberg, S. L. Fast gapped-read alignment with Bowtie 2. *Nat Methods*
964 **9**, 357–359 (2012).
965 120. Li, H. *et al.* The Sequence Alignment/Map format and SAMtools. *Bioinformatics* **25**, 2078–
966 2079 (2009).
967 121. GitHub - jsh58/Genrich: Detecting sites of genomic enrichment.
968 https://github.com/jsh58/Genrich.
969 122. Robinson, M. D., McCarthy, D. J. & Smyth, G. K. edgeR: a Bioconductor package for
970 differential expression analysis of digital gene expression data. *Bioinformatics* **26**, 139–140
971 (2010).

123. Chen, Y., Chen, L., Lun, A. T. L., Baldoni, P. L. & Smyth, G. K. edgeR 4.0: powerful differential analysis of sequencing data with expanded functionality and improved support for small counts and larger datasets. 2024.01.21.576131 Preprint at https://doi.org/10.1101/2024.01.21.576131 (2024).

124. Lun, A. T. L. & Smyth, G. K. csaw: a Bioconductor package for differential binding analysis of ChIP-seq data using sliding windows. *Nucleic Acids Res* **44**, e45 (2016).

125. Ashuach, T. *et al.* MPRAnalyze: statistical framework for massively parallel reporter assays. *Genome Biology* **20**, 183 (2019).

126. Bao, L., Zhou, M. & Cui, Y. CTCFBSDB: a CTCF-binding site database for characterization of vertebrate genomic insulators. *Nucleic Acids Research* **36**, D83–D87 (2008).

127. Ziebarth, J. D., Bhattacharya, A. & Cui, Y. CTCFBSDB 2.0: a database for CTCF-binding sites and genome organization. *Nucleic Acids Research* **41**, D188–D194 (2013).

128. Bailey, T. L. & Grant, C. E. SEA: Simple Enrichment Analysis of motifs. 2021.08.23.457422 Preprint at https://doi.org/10.1101/2021.08.23.457422 (2021).

129. Wu, T. *et al.* clusterProfiler 4.0: A universal enrichment tool for interpreting omics data. *The Innovation* **2**, 100141 (2021).

130. Pickrell, J. K. *et al.* Detection and interpretation of shared genetic influences on 42 human traits. *Nat Genet* **48**, 709–717 (2016).

131. Giambartolomei, C. *et al.* A Bayesian framework for multiple trait colocalization from summary association statistics. *Bioinformatics* **34**, 2538–2545 (2018).

132. Gamazon, E. R. *et al.* A gene-based association method for mapping traits using reference transcriptome data. *Nature Genetics* **47**, 1091–1098 (2015).

133. Barbeira, A. N. *et al.* Exploring the phenotypic consequences of tissue specific gene expression variation inferred from GWAS summary statistics. *Nature Communications* **9**, 1–20 (2018).

997

998

999

1000 **Figure 0. Schematic.** Made with BioRender

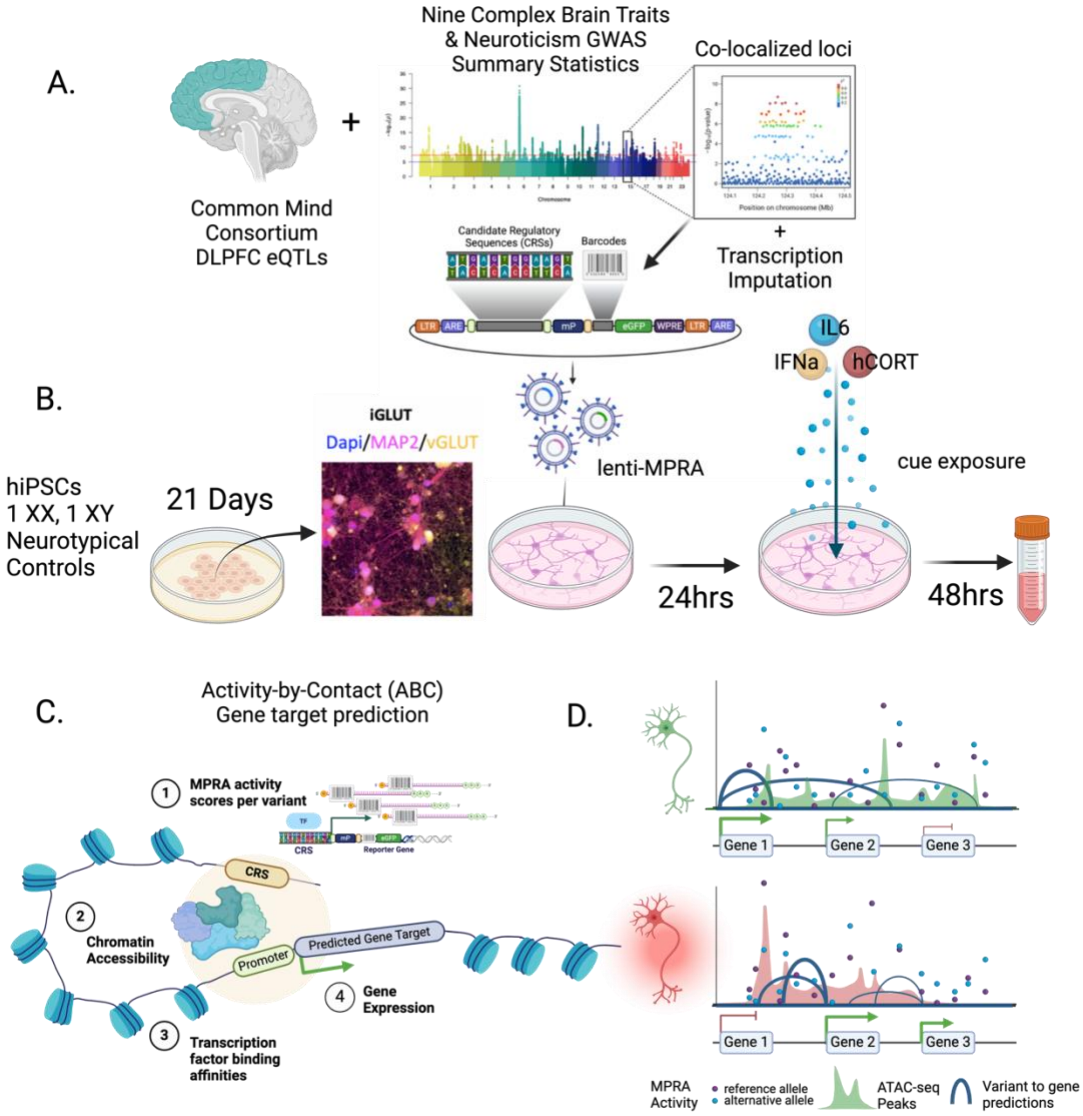

1001

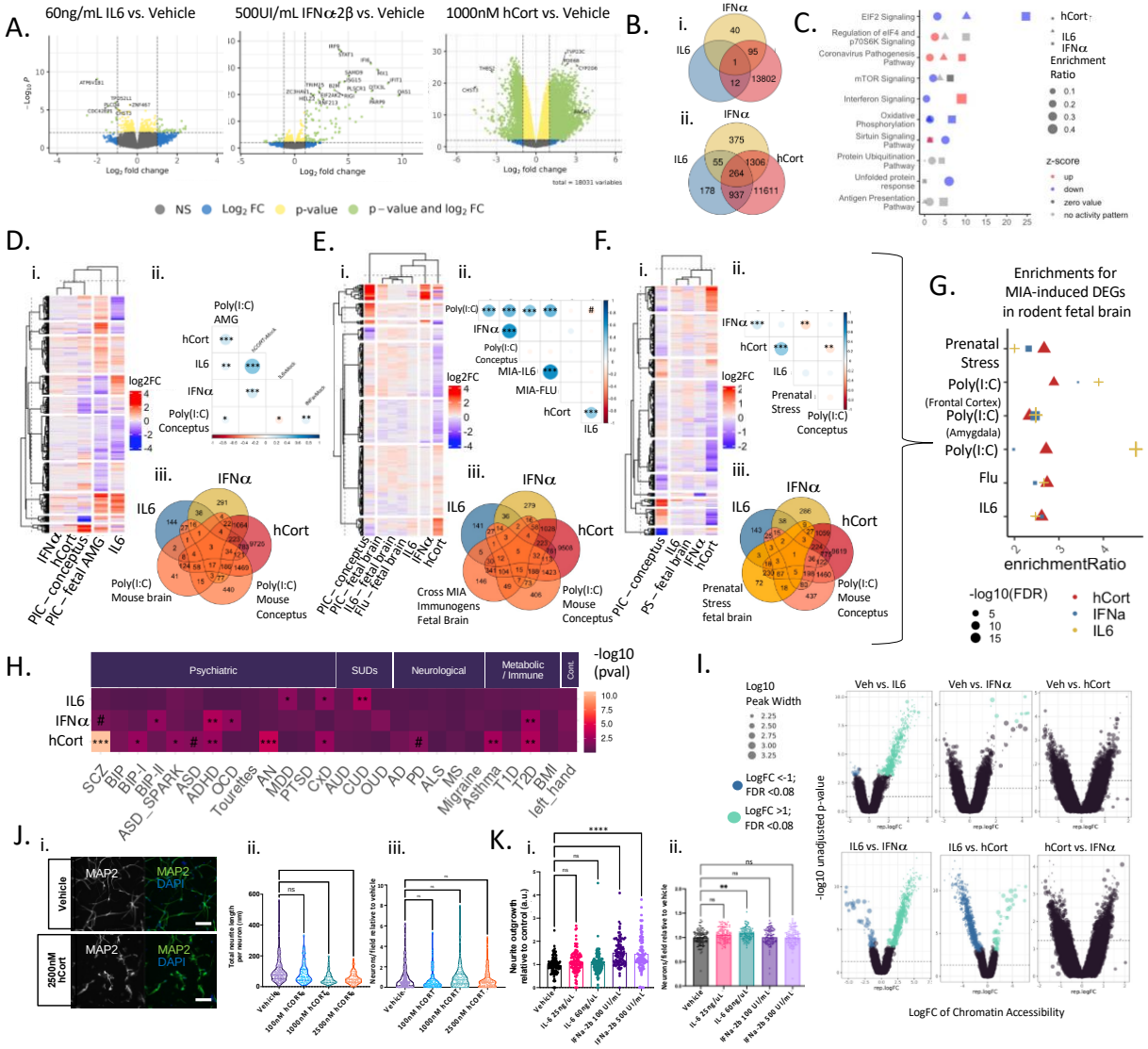

Figure 1. Stress and inflammatory factors impacted gene expression, chromatin accessibility, cell morphology, but not survival, in developing neurons. Differential gene expression analysis in iGLUTs exposed to 1000nM hCort, 60ng/uL IL-6, or 500 UI/mL IFNa-2b (compared to vehicle) revealed unique and shared effects on the transcriptome. **(A)** 1000nM hCort resulted in transcriptomic-wide dysregulation, while the effects of 60ng/mL IL-6 produced moderate downregulation of few genes, and IFNa-2b resulted in strong upregulation of select immune-related genes. **(B)** Overlapping **(i)** significant (FDR<0.05) and **(ii)** nominally significant (unadjusted p-value<0.05) DEGs by cue. **(C)** Signed pathway enrichment of cue-specific transcriptomic dysregulation (DEGs; unadjusted p-value<0.05) (**Supplemental Data 2**). **(D-F)** Gene expression changes in the mouse amygdala, frontal cortex, and whole brain following Poly(I|C), IL6, or *H1N1*-induced MIA significantly correlated with transcriptomic signatures of IL-6 and hCort**. (i)** Heatmap of log2FC across shared genes. **(ii)** Pearson's correlation of log2FC across cue-exposures and MIA-induced mouse brain DEGs (# = FDR<0.08; * = FDR<0.05; ** = FDR<0.01; *** = FDR<0.001). (**iii**) Overlap of nominal significantly different DEGs and MIA-induced mouse brain DEGs **(G)** Enrichment of cue-specific dysregulation (DEGs; unadjusted p-

value<0.05) for MIA-induced fetal brain DEGs across MIA rodent models. **(H)** Enrichment of cue-specific transcriptomic dysregulation (DEGs; unadjusted p-value<0.05) for GWAS risk genes across psychiatric, neurological, and immune traits. # = FDR<0.08; * = FDR<0.05; ** = FDR<0.01; *** = FDR<0.001. **(I)** Differential peak accessibility analysis in iGLUTs exposed to 1000nM hCort, 60ng/uL IL-6, or 500 UI/mL IFNa-2b (compared to vehicle) showed significant decreases in chromatin accessibility following exposure to IL-6. **(J)** Dose-dependent impact of exposure of hCort, IL-6, and IFNa-2b on early (D7) neurite outgrowth in iGLUTs. **(i-iii)** Exposure of 1000nM and 2500nM hCort significantly decreased early neurite outgrowth while exposure to **(K) (i-iii)** 100 UI/mL and 500 UI/mL IFNa-2b increased neurite outgrowth, relative to vehicle control conditions. N = minimum of 2 independent experiments across 2 donor lines with 12 technical replicates per condition and 9 images analyzed per replicate. One way ANOVA with post-hoc Bonferroni multiple comparisons test. * = p<0.05; ** = p<0.01; *** = p<0.001; **** = p<0.0001.

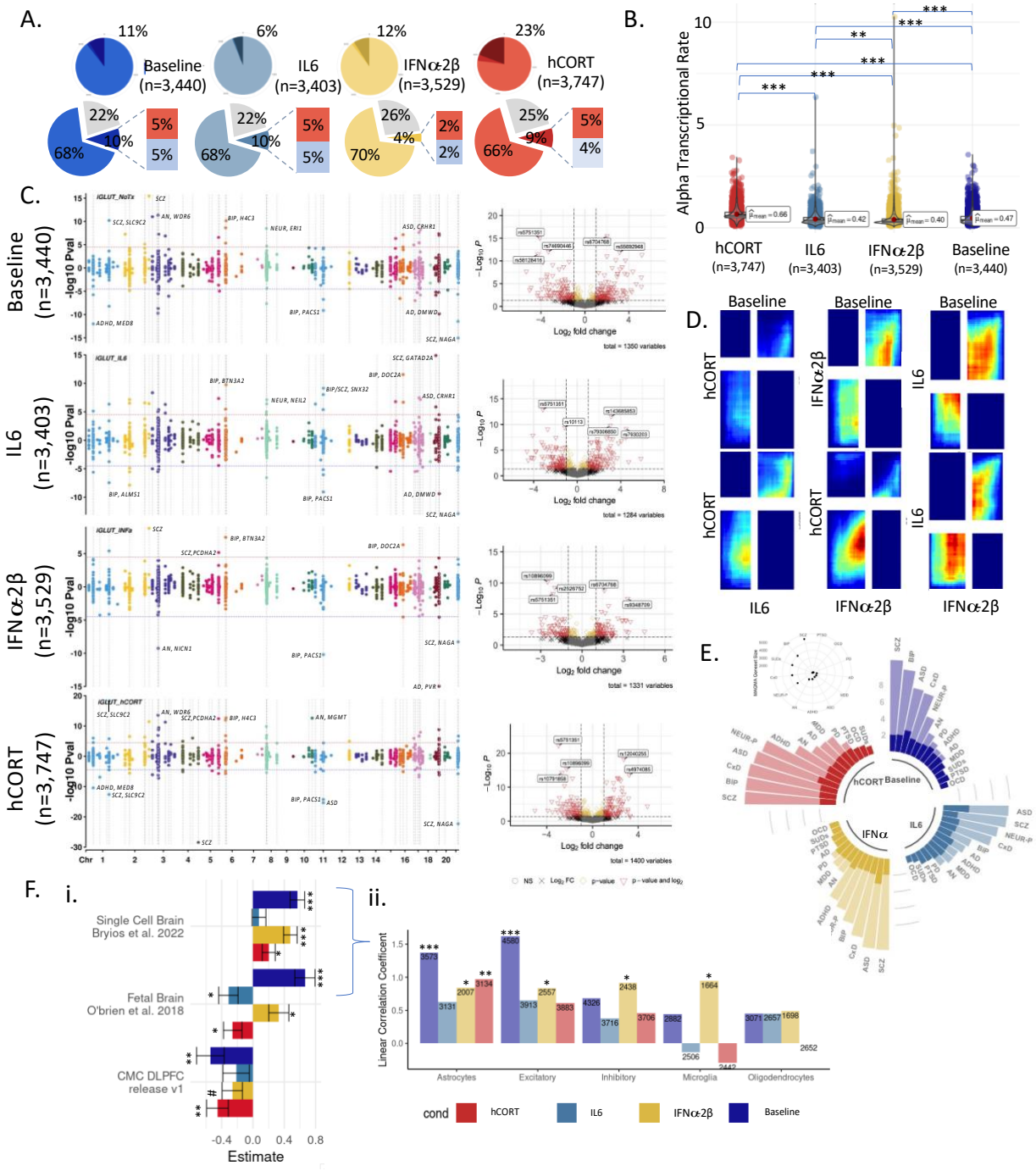

Figure 2. Inflammatory and stress factors altered allele-specific regulatory activity of risk-CREs and were uniquely enriched for psychiatric disorders. (A) ~3440 variants were captured and tested at baseline, with an average transcriptional activity of 11%. The average percent of significantly active candidate regulatory elements (CRE) varied by cue exposure. Top circle represents the proportion of significantly active CRE (FDR<=0.1) across conditions (dark blue=baseline, teal=IL-6, golden yellow=IFNa-2B, red=hCort). **(B)** Exposure to different cues resulted in significantly different levels of mean transcriptional activity across all CRE tested, with hCort resulting in the largest increase in mean-transcriptional rate. **(C)** Top allelic shifts by

disorder, locus, and SNP showed dynamic cue-specific effects on genetic regulation. Manhattan plots of differential allelic shifts (ref vs. alt) across cue-exposures with loci labeled by PrediXcan/Coloc2 associated disorder eGenes. Each point represents an individual tested SNP at a given locus with chromosome location on the x-axis and the signed -log10 p-value of differential transcriptional activity between the reference and alternative alleles on the y-axis. Volcano plots demonstrate allelic shifts (ref vs. alt) across cue-exposures labeled by top SNPs. **(D)** Rank-rank hypergeometric test of transcriptional activity across cues: IL6 exposure is most highly correlated with activity at baseline, while hCORT exposure is the least correlated. **(E)** Significant CRE show cue-biased enrichments for GWAS risk SNPs across psychiatric disorders, scaled and ordered by -log10 (FDR). **(F) (i)** Enhancer activity of regulatory elements tested in iGLUTs are significantly positively correlated with brain single cell and the fetal postmortem brain eQTL effects, but significantly negatively correlated adult DLPFC eQTL effects. **(ii)** Linear coefficients of single cell eQTLs with MPRA activity by cell-type shows that, at baseline, activity of CREs significantly recapitulates eQTL effects in excitatory neurons, while IFNa and hCORT exposure recapitulate effects in astrocytes, and IFNa exposure uniquely recapitulates these effects in microglia. Bar chart of linear correlation coefficients of eQTL betas [abs(MPRA allelic shift) ~ abs(eQTL Beta) + log distance to the transcriptional start site + Gene/Transcript + CellType]. (FDR<=0.08$^{\#}$, FDR<0.05*, FDR<0.01**, FDR<0.001***).

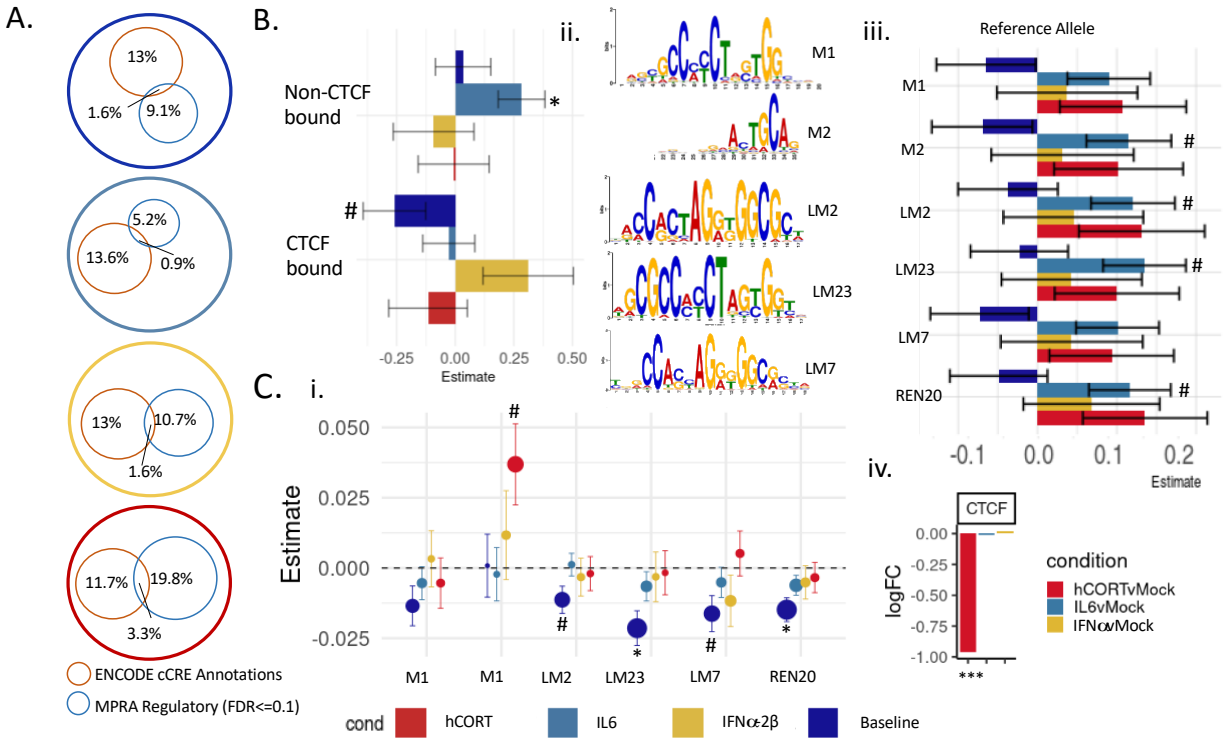

Figure 3. CTCF binding negatively influenced transcriptional activity in a cue-specific manner. Baseline activity of CTCF-bound sequences was significantly reduced related to non-CTCF-bound regions (**SI Figure 6**). **(A)** Percent overlap between MPRA CRE with known ENCODE cCRE annotations (orange circle) and significantly active CRE (FDR<0.1) (blue circle). Active MPRA CRE were not enriched for ENCODE cCREs, with only 1-3% previously annotated as regulatory elements. The proportion of active MPRA CRE overlapping with known proximal or distal enhancer- or promoter-like sequences shifted with exposure to stress and inflammatory factors. **(B)** Linear correlation coefficients for CTCF-binding showed significant negative correlations of CTCF binding enhancer-like regions at baseline, and a significantly positive association of non-CTCF bound enhancer-like regions with IL-6-responsive activity (MPRA Median Z-score ~ CTCFe + nonCTCF + nonoverlap) **(C)** Six highly conserved core CTCF binding motifs best match active CRE sequences (**Supplemental Data 1**). **(i)** At baseline, motif scores for two (LM7, LM2) were nominally and two (LM23, REN30) were significantly negatively associated with transcriptional activity. A separate motif (M1) was nominally positively associated with transcriptional activity after hCort exposure**. (ii)** Motif logos of five highly conserved CTCF binding motifs tested in (i). **(iii).** Linear coefficients for allele effects. **(iv)** CTCF is significantly downregulated following exposure to 1000nM in iGLUTs. (MPRA median z-score ~ CTCF motif score + orientation + allele + distance from center SNP + motif; estimates for orientation are reported in **SI Figure 8**). (FDR<=0.08$^{\#}$, FDR<0.05*, FDR<0.01**, FDR<0.001***).

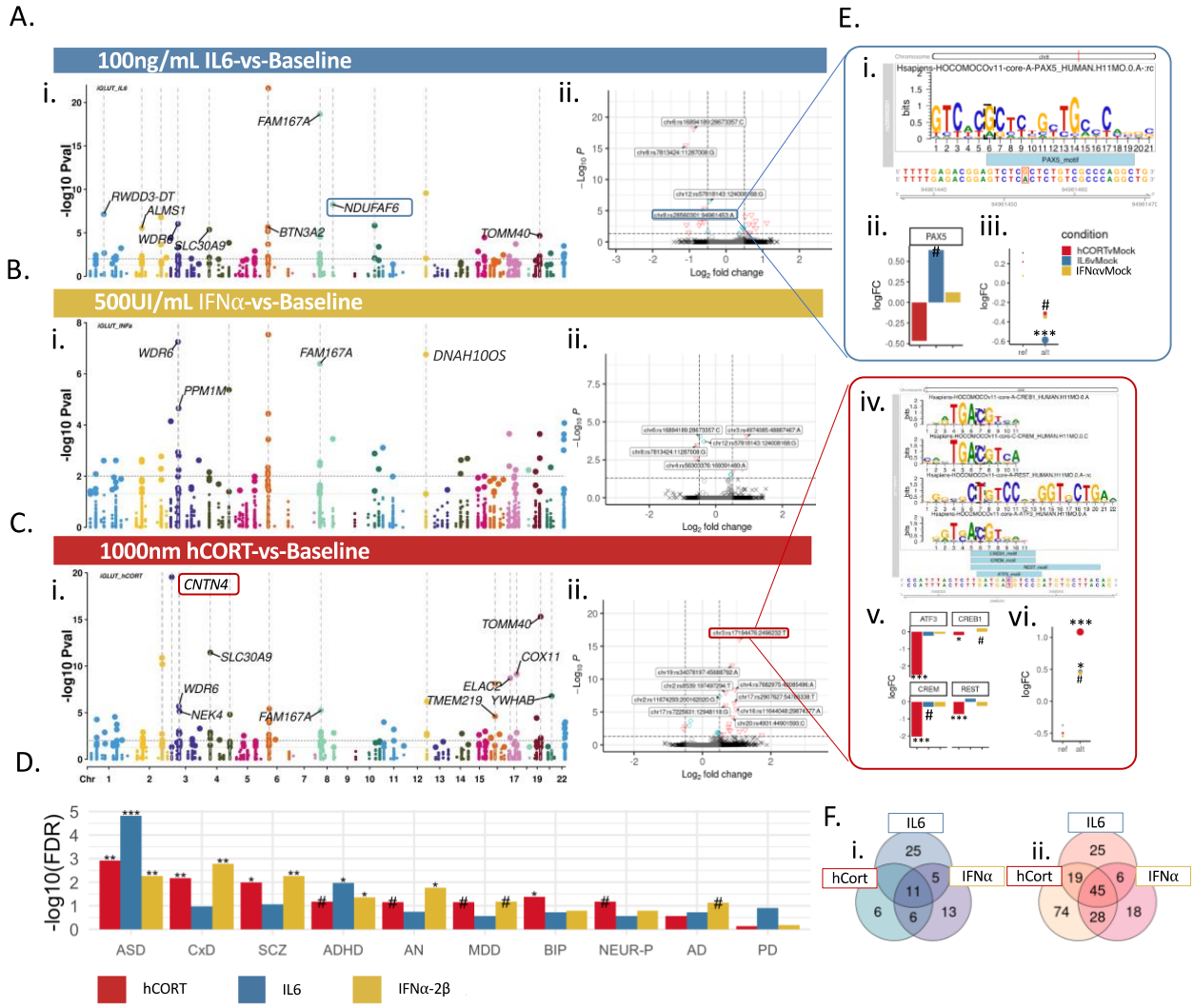

Figure 4. Cue-specific differences in active CREs were driven by transcription factor binding affinities. Stress and inflammatory factors dynamically and specifically impacted allelic shifts in transcriptional activity of CREs in iGLUTs. **(A-C)** Manhattan plots of differentially active CREs between each cue-exposure and baseline labeled by PrediXcan associated disorder and eGenes. Each point represents an individual tested SNP at a given locus with chromosomal location on the x-axis and the -log10 p-value of differential transcriptional activity between cue-exposure and baseline on the y-axis. **(D)** Differentially active CRE enrichments across GWAS psychiatric disorder and neurodegenerative disease risk SNPs. For each cue exposure, different disorders showed top enrichments (FDR<=0.08$^{\#}$, FDR<0.05*, FDR<0.01**, FDR<0.001***). **(E)** Motif-binding was significantly impacted by variant shifts at SNPs with cue-specific responses. Example of two SNPs with cue-by-variant specific effects with variant-specific TF binding affinities: (i) MotifBreaker image of the regulatory sequence centered at rs28560301 in the AD-associated *NDUFAF6* locus, showing PAX5, which has decreased predicted binding affinity with the risk allele. (ii) Cue-specific differential gene expression; *PAX5* expression is increased following IL-6 exposure. (iii) Cue-specific difference in CRE activity compared to baseline of represented SNP; rs28560301 risk allele is significantly decreased follow IL-6 exposure compared to baseline. (iv) Transcriptional activators (CREB, CREM, ATF3) have increased binding affinities for the reference allele, while REST, a master transcriptional silencer, has increased binding to

the risk allele. (v) CREB, CREM, ATF3, and REST were significantly downregulated following hCort exposure. (vi) SCZ-associated alternative allele (rs1719446) were significantly more active following hCort exposure. **(F)** Venn diagram of overlapping nominally significant (p-value<=0.05) CRE with increased activity (i) or decreased activity (ii) by condition.

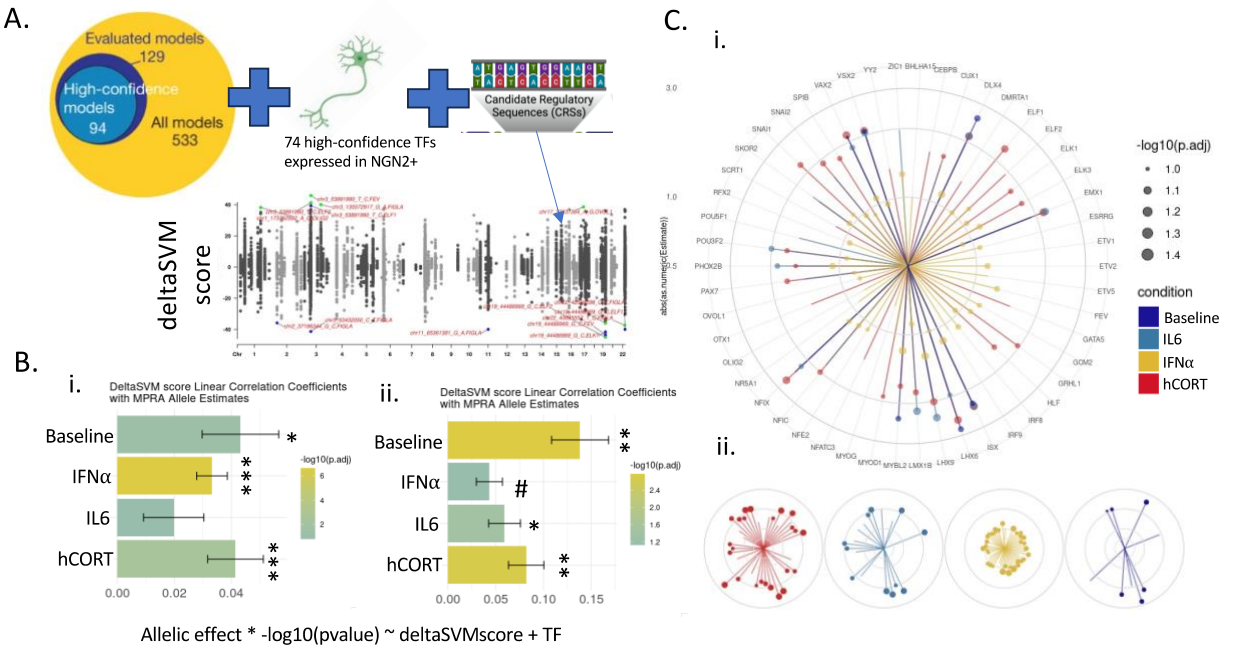

Figure 5. Variant-specific changes in transcription factor binding affinities predicted cue-specific allelic shifts in transcriptional activity. (A) DeltaSVM quantifies the effect of single nucleotide sequence changes on transcription factor binding activity. Using 74 high-confidence TFs (Yan et al. 2021[69]) expressed in iGLUTs, DeltaSVM scores were calculated for each CRE. Manhattan plot of deltaSVM scores for each CRE comparing reference to alternative allele. **(B)** DeltaSVM scores significantly positively correlated with allele-specific activity quantified in the MPRA. DeltaSVM score linear correlation coefficients with MPRA allelic shifts **(i)** before and **(ii)** after restricting to regions with predicted allelic preference by deltaSVM (Allelic effect * -log10(pvalue) ~ deltaSVMscore + TF model). **(C**) Specific TF binding affinities model predicted allele-specific activity by exposure. **(i)** TF linear correlation coefficients by condition. Circular segments represent the absolute value of TF-factor specific linear correlation coefficients, the size of the dot represents the -log10 FDR of the estimate. Colors indicate cue-specific activity (dark blue=Baseline, teal = IL-6, golden yellow=IFNa-2b, dark red=hCort). **(ii)** TF binding affinities explain, in part, cue specific changes in transcriptional activity. (FDR<=0.08[#], FDR<0.05[*], FDR<0.01[**], FDR<0.001[***]).

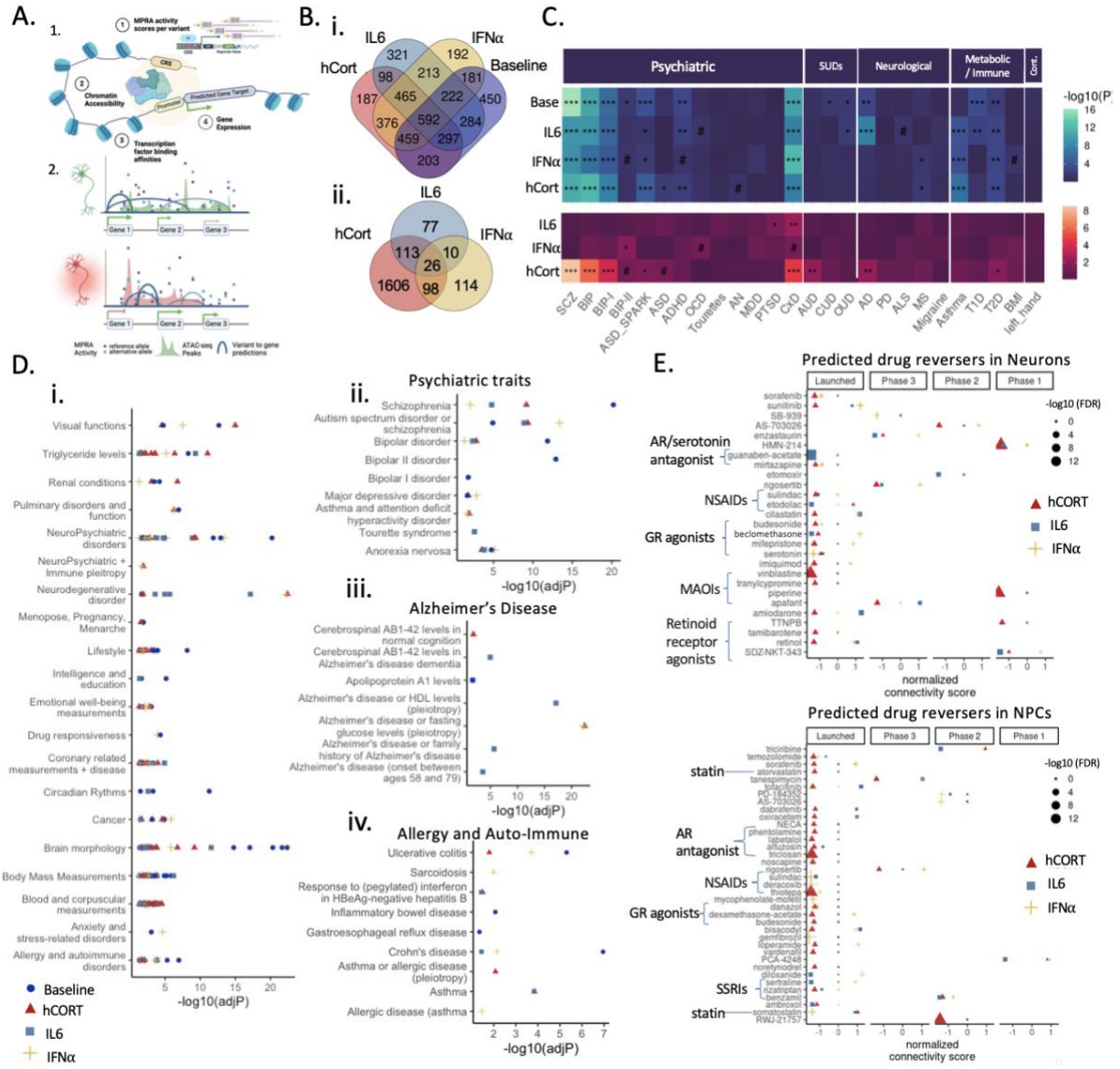

Figure 6. Gene targets of context-specific regulatory elements showed distinct associations with brain disorders and medications. (A) Workflow of activity-by-contact enhancer-gene interaction scoring (made with BioRender). (1.) By integrating cell type and cue-specific MPRA enhancer activity, cell and cue-specific chromatin accessibility, and transcription factor binding affinities we (2.) predict cell-type and cue-specific genetically regulated genes (ABC genes) **(B)** Predicted ABC gene targets of active CREs across cues. Venn diagrams of overlapping ABC genes mapped to **(i)** active significantly enhancers across cue-exposures (FDR<0.1) and to **(ii)** differentially active CRE (nominal p-value <=0.05) by cue compared to baseline. **(C)** MAGMA enrichment analysis across psychiatric, substance use (SUD), neurological, and metabolic/immune disorders revealed unique association of cue specific genetically regulated genes with disorder risk. **(D)** GWAS catalogue over representation analysis **(i)** identified unique and shared trait enrichment across cues, including enrichments for psychiatric **(ii)**, neurodegenerative **(iii)**, and allergy/autoimmune enrichments **(iv) (Supplemental Data 2)**.

(E) Cue-specific ABC target genes resolved shared and unique drug reversers. (FDR<=0.08$^{\#}$, FDR<0.05*, FDR<0.01**, FDR<0.001***).

EXTENDED DATA

Supplemental Table 1. GWAS studies used to prioritize cross-psych MPRA library.

Supplemental Table 2. Number of prioritized SNPs by colocalization (Coloc2) across GWAS.

Supplemental Table 3. Number of prioritized SNPs by S-PrediXcan across GWAS.

Supplemental Table 4. Number of captured CRE with sufficient barcodes across MPRA.

Supplemental Figure 1. Selection of predicted cis-expression quantitative trait loci (*cis*-eQTLs).

Supplemental Figure 2. Design of cross-disorder MPRA library.

Supplemental Figure 3. Stress and inflammatory factors associated with MIA significantly dysregulated the transcriptomic in developing iGLUTs.

Supplemental Figure 4. Stress and inflammatory factors altered neurite outgrowth in hiPSC-derived iGLUTs.

Supplemental Figure 5. Correlation between MPRA experimental replicates.

Supplemental Figure 6. Correlation between MPRA donors and contexts.

Supplemental Figure 7. Stress and inflammatory factors uniquely impacted allelic-specific transcriptional activity of CRE in iGLUTs.

Supplemental Figure 8. Transcription factor binding motifs were differentially enriched in active CRE based on context.

Supplemental Figure 9. CTCF binding, but not chromatic accessibility measures, influenced cue-specific MPRA allelic shifts.

Supplemental Figure 10. Predicted TF binding SNP regulatory effects correlated significantly with MPRA allelic shifts.

Supplemental Figure 11. Expression of TFs predicted to regulate cue-specific MPRA activity.

Supplemental Figure 12. Cue-specific impacts on biological pathways.

Supplemental Table 2. GWAS studies used to prioritize cross-psych MPRA library.

GWAS	Year	Study	Genome Ref	N	Ncases	Ncontrols
AD	2019	Marioni et al. 2019	NCBI Build 37/UCSC hg19	388324	74046	314278
ADHD	2018	Demontis et al. 2018	NCBI Build 37/UCSC hg19	55374	20183	35191
AN	2019	Watson et al. 2019	NCBI Build 37/UCSC hg19	72517	16992	55525
ASD	2019	Grove et al. 2019	NCBI Build 37/UCSC hg19	46351	18382	27969
BIP	2021	Mullins et al 2021	NCBI Build 37/UCSC hg19	413466	41917	371549
SCZ	2022	Trubetskoy et al. 2022	NCBI Build 37/UCSC hg19	161405	67390	94015
OCD	2018	Arnold et al. 2018	NCBI Build 37/UCSC hg19	9725	2688	7037
MDD	2019	Howard et al. 2019	NCBI Build 37/UCSC hg19	142646	45396	97250
PTSD	2020	Huckins et al. 2020	NCBI Build 37/UCSC hg19	200000	30000	170000
NEUR	2017	Lo et al. 2017	NCBI Build 37/UCSC hg19	59206	NA	NA

Supplemental Table 2. Number of prioritized SNPs by colocalization (Coloc2) across GWAS.

Disorder	#loci (1e-6)	#Genes w/ >= 1 cis-eQTL FDR <0.05	#co-localized loci	Unique Causal SNPs	#Causal + LD snps
AD	49	162	10	10	25
ADHD	52	85	15	12	64
AN	41	68	1	1	1
ASD	26	71	14	13	94
BIP	195	500	45	36	125
SCZ	482	772	40	34	84
OCD	56	125	2	1	8
MDD	31	112	7	7	29
PTSD	7	4	2	2	7
NEUR	15	38	0	0	0
Total	**954**	**1937**	**136**	**116**	**437**
# Total SNPs accounting for overlap					**429**
P-value Threshold for sig. snps		**<=1e^-6**			
PPH4 Threshold for DLPFC coloc2		**>0.5**			
High LD Threshold		**r^2 >= 0.9**			

Supplemental Table 3. Number of prioritized SNPs by S-PrediXcan across GWAS.

Disorder	MetaXcan GWSig Genes (p<=0.00005)	# gene snps	LD snps >=0.8	# gene + LD snps
AD	12	222	319	541
ADHD	4	118	300	418
AN	5	128	445	573
ASD	4	16	8	24
BIP	26	655	1430	2085
MDD	4	90	462	552
NEUR	19	420	626	1046
OCD	0	0	0	0
PTSD	0	0	0	0
SCZ	43	1101	1758	2859
TOTAL	**116**	**2750**	**5348**	**8098**
# Total SNPs after accoutning for overlap and filtering for LD r^2>=0.9				**4068**
P-value Threshold for DLPFC MetaXcan:		**0.05/10786**	**4.63564E-06**	
High LD Threshold	**r^2 >= 0.9**			

Supplemental Table 4. Number of captured CRE with sufficient barcodes across MPRA.

Donor	Tx	Replicate	Total CRS	Portion of Total CRS	mean nbarcodes	median n barcodes	CRS >= 10 bcs	Portion of Total CRS	rep1-2_RNA	rep1-2_DNA	rep1-2_Ratio_corr
2607	Baseline	1	6749	87.5%	10.5	5					
2607	Baseline	2	6697	86.8%	11	4			1	0.99	0.32
3182	Baseline	1	6613	85.7%	10.14	4					
3182	Baseline	2	6557	85.0%	9.95	4	3440	44.6%	1	0.99	0.65
2607	1000nM hCort	1	6667	86.4%	10.5	5					
2607	1000nM hCort	2	6639	86.1%	10.7	4			1	1	0.53
3182	1000nM hCort	1	6384	82.8%	9.8	4					
3182	1000nM hCort	2	6724	87.2%	10.8	5	3747	48.6%	1	0.99	0.46
2607	60ng/uL IL6	1	6480	84.0%	9.8	4					
2607	60ng/uL IL6	2	6636	86.0%	10.4	4			1	1	0.57
3182	60ng/uL IL6	1	6639	86.1%	10.1	4					
3182	60ng/uL IL6	2	6536	84.7%	9.6	4	3403	44.1%	1	1	0.66
2607	500UI INFa-2b	1	6605	85.6%	10.1	4					
2607	500UI INFa-2b	2	6161	79.9%	9.2	3			0.99	0.99	0.21
3182	500UI INFa-2b	1	6683	86.6%	10.5	5					
3182	500UI INFa-2b	2	6670	86.5%	10.3	4	3529	45.7%	1	1	0.67
Note:	Designed Library A contained 7714 CRS with at least 10 barcodes (83% of the original library)										

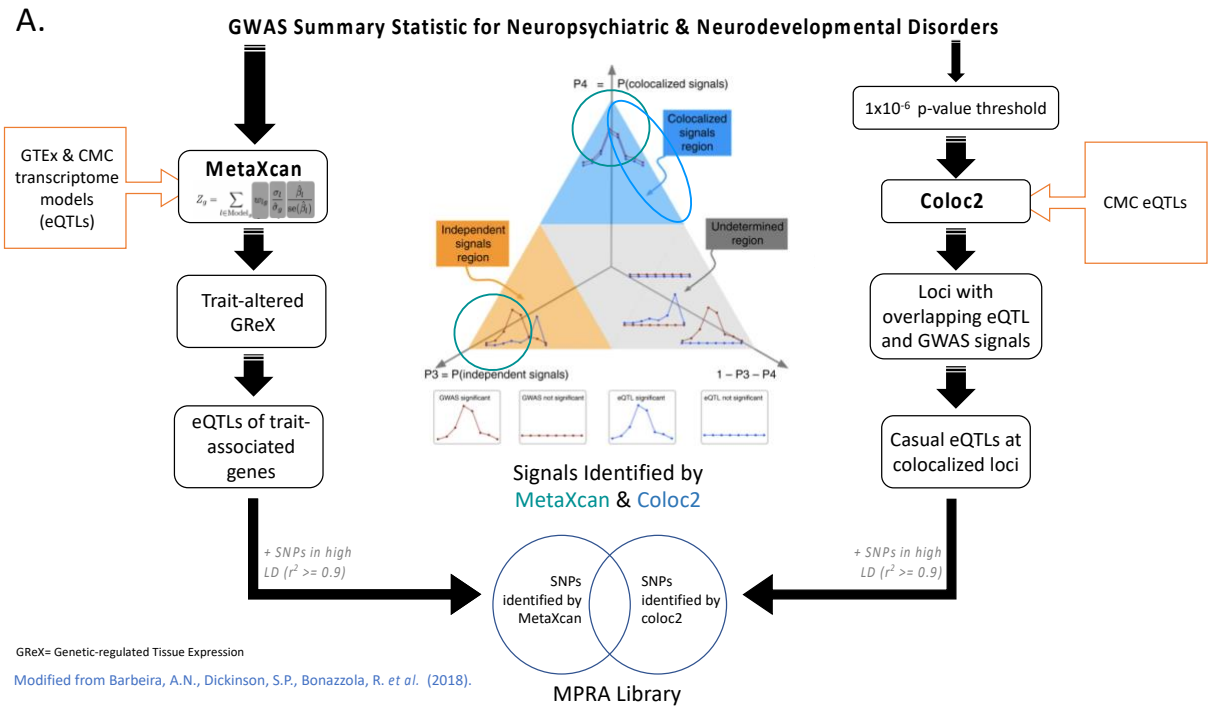

Supplemental Figure 8. Selection of predicted cis-expression quantitative trait loci (*cis*-eQTLs). Variant selection for inclusion in the library was based nine GWAS (AD, ADHD, AN, ASD, BIP, MDD, PTSD, SCZ, and NEU) using two selection approaches: (1) Bayesian co-localization (using coloc2[130,131]) and (2) transcriptomic imputation (S-PrediXcan[132,133]) (**Figure 6**). For method 1, significant GWAS loci were identified based on an LD $r^2 > 0.1$ with the lead associated SNPs ($p<1x10^{-6}$). Overlapping loci were merged. Genes that overlapped with these loci and had one or more CMC DLPFC cis-eQTLs (FDR < 0.05) were tested for co-localization using coloc2[131]. Loci with PPH4 >= 0.5 were considered moderately to strongly co-localized. The most probable causal eQTLs from these loci were selected, along with all SNPs in high LD (r^2 >= 0.8). For method 2, trait-associated CMC DLPFC S-PrediXcan genes ($p<\sim4.64x10^{-6}$ (0.05/10786)) were selected for AD, ADHD, AN, ASD, BIP, MDD, PTSD, and SCZ, and NEU. All SNPs within the predictor models of significant genes (3-15/gene) and all SNPs in high LD (r^2 >= 0.8) with them were selected. 100 positive and 100 negative controls were selected from SNPs (i) producing the 100 greatest and 100 least transcriptional shifts based on a previous SCZ and AD MPRA[115] and (ii) present in the CMC DLPFC dataset. Additional negative controls were selected from significant BIP GWAS loci that (i) did not colocalize (PPH4 < 0.1) and (ii) were not significant CMC DLPFC eQTLs. While our methods for identification were expression-based and greatly differed from the MPRA used to select the controls, four positive controls were also identified by our methods (**Supplemental Data 1**).

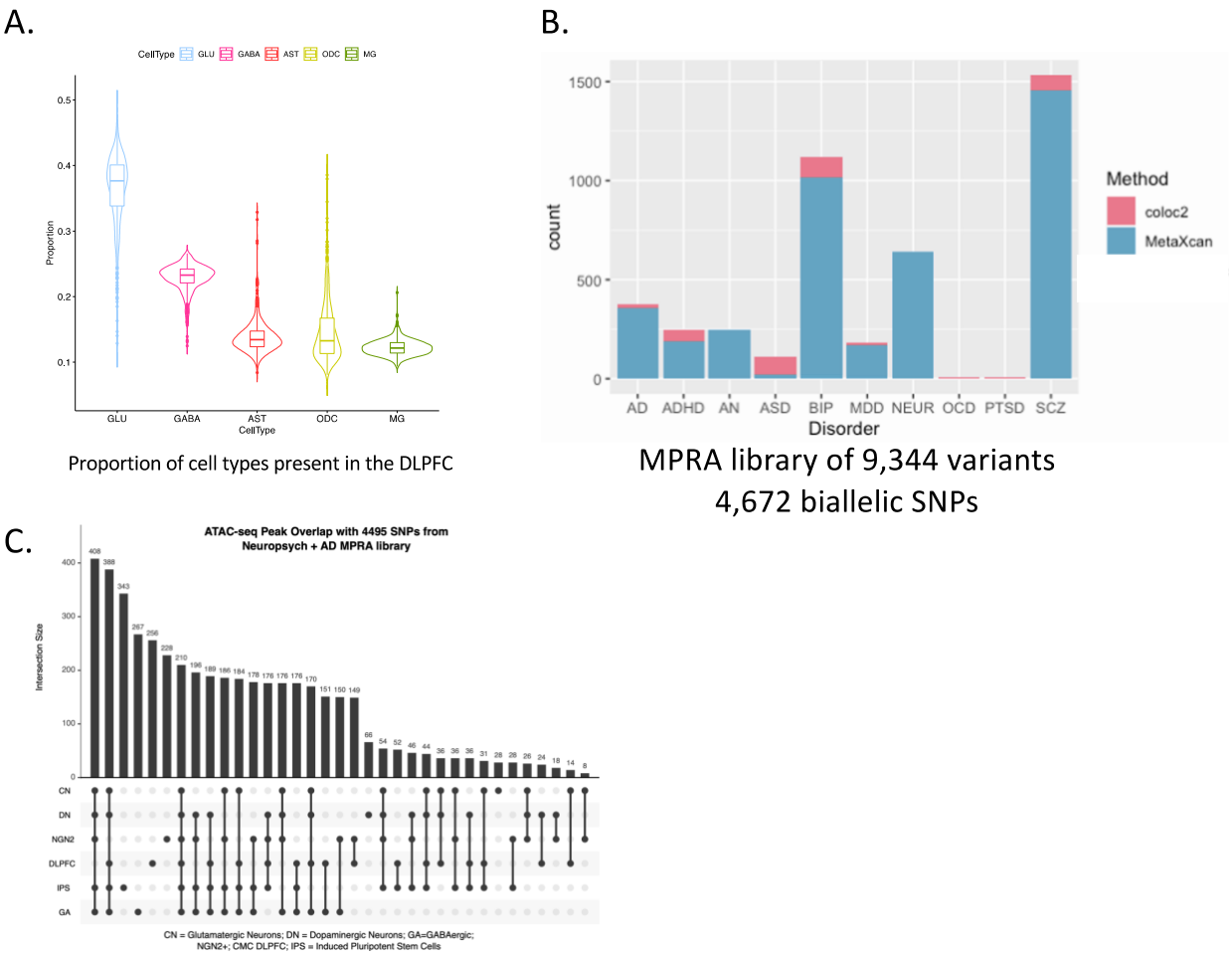

Supplemental Figure 9. Design of cross-disorder MPRA library. **(A)** Estimate proportion of cell types present in the CMC postmortem dorsolateral prefrontal cortex (DLPFC) by cell-type deconvolution. **(B)** Proportion of test SNPs by prioritization method and GWAS summary statistics. **(C)** Level of ATAC-seq peak overlap with putative CRE by cell-type. (CN=glutamatergic, DN=dopaminergic, GA=GABAergic, NGN2=hiPSC-derived NGN2 iGLUTs, iPS=human-induced pluripotent stem cell).

A.

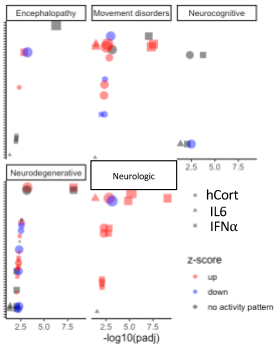

B.

	Cues	Het. FDR	Dir.	nGenes
Dynamic	hCort, IL6, IFNα	<=0.05	+	2168
			-	3226
Stable	hCort, IL6, IFNα	>=0.05	+	352
			-	258
	hCort + IL6	>=0.05	+	65
			-	24
	hCort + IFNα	>=0.05	+	53
			-	44
	IL6 + IFNα	>=0.05	+	5
			-	3

Meta-analyzed significantly differentially expressed genes (meta FDR adjusted p-value <=0.05)

C.

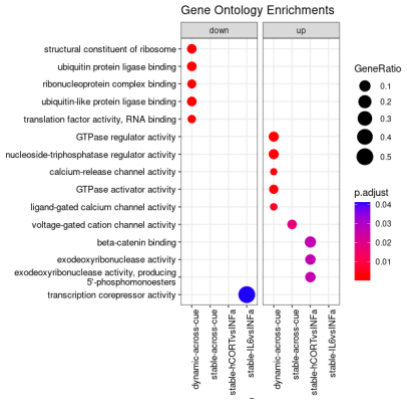

D.

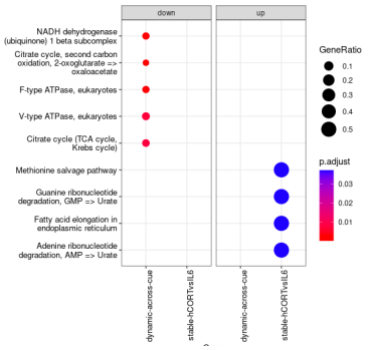

E.

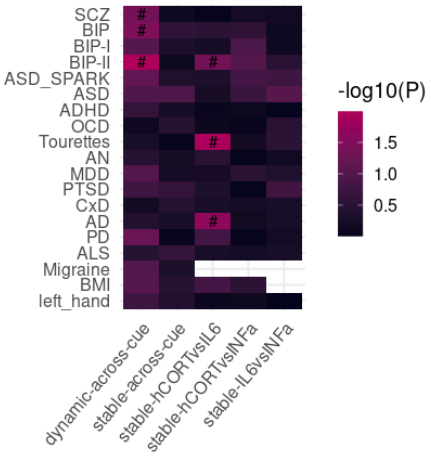

Supplemental Figure 10. Stress and inflammatory factors associated with MIA significantly dysregulated the transcriptomic in developing neurons. Differential gene expression analysis in iGLUTs exposed to 1000nM hCort, 60ng/uL IL-6, or 500 UI/mL IFNa-2B (compared to vehicle) revealed unique and shared effects of these cellular stressor on the transcriptome (**Figure 2.1**). **(A)** Signed pathway enrichment of cue-specific transcriptomic dysregulation across brain disorders highlight unique contributes to risk. **(B)** Meta-analysis across conditions identified both dynamic and stable changes in gene expression. Across all conditions, 258 were consistently downregulated and 352 consistently upregulated, 65 upregulated DEGs and 24 down regulated DEGs uniquely shared between hCort and IL-6 treatment, 53 upregulated DEGs and 44 downregulated DEGs were s uniquely shared between hCort and IFNa-2b, and 5 upregulated and 3 downregulated DEGs were uniquely shared between IL-6 and IFNa-2b (Meta adjusted p-value <= 0.05; Cochran's Heterogeneity p-value >=0.05). **(C-D)** Biological theme comparison between gene clusters revealed significant negative enrichment in transcription corepressor activity in DEGs unique to IL-6 and IFNa, significant positive enrichments in beta-catenin binding and exodeoxyribonuclease activity in DEGs unique to hCort and IFNa-2b, and significant positive enrichment for ribonucleotide degradation and fatty acid elongation in the ER for DEGs unique to IL-6 and hCort. Shared DEGs across all conditions were positively enriched for voltage-gated cation channel activity. **(E)** MAGMA GWAS enrichment for meta-analyzed categories (# pvalue <= 0.05) (related to **Figure 1; Supplemental Data 2**).

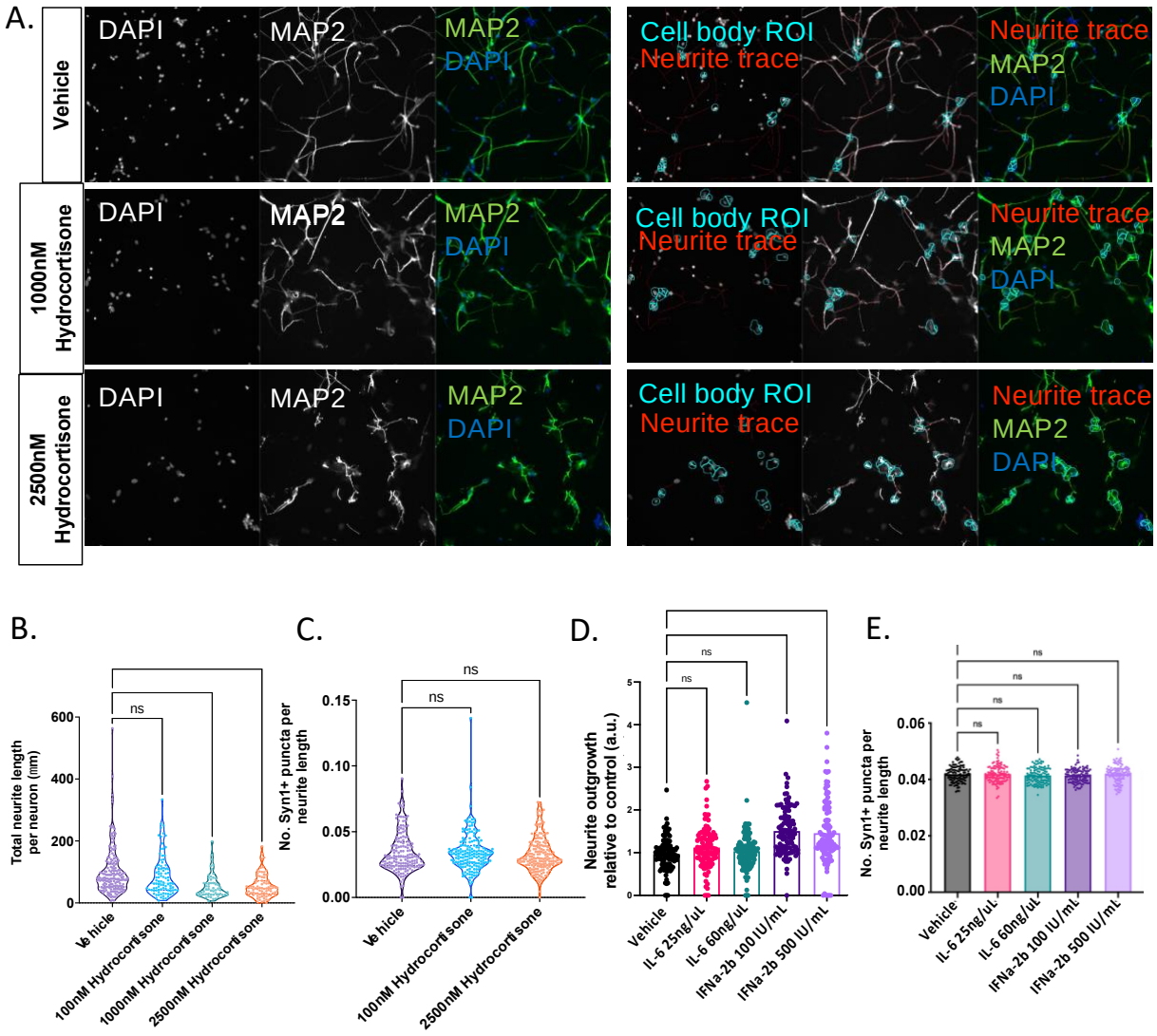

Supplemental Figure 11. Stress and inflammatory factors altered neurite outgrowth in hiPSC-derived neurons. Representative images and neurite traces demonstrating the impact of 48hr exposure of hydrocortisone (hCort), IL-6, and I-2b across multiple doses on early (D7) neurite outgrowth in hiPSC-derived iGLUTs and perturbations on Synapsin1 (Syn1) +ve puncta expression in D21 hiPSC-derived iGLUTs. Syn1+ve puncta values are expressed relative to MAP2 +ve neurite length in each image. **(A, B)** Exposure of 1000nM and 2500nM resulted in significant decreases in early neurite outgrowth while exposure to **(D)** 100 UI/mL and 500 UI/mL IFNa-2b increased neurite outgrowth relative to vehicle control conditions. **(C,E)** Synaptic puncta density was not affected by cue-exposure. N = minimum of 2 independent experiments across 2 donor lines with 12 technical replicates per condition and 9 images analyzed per replicate. One way ANOVA with post-hoc Bonferroni multiple comparisons test (related to **Figure 1**). * = p<0.05; ** = p<0.01; *** = p<0.001; **** = p<0.0001.

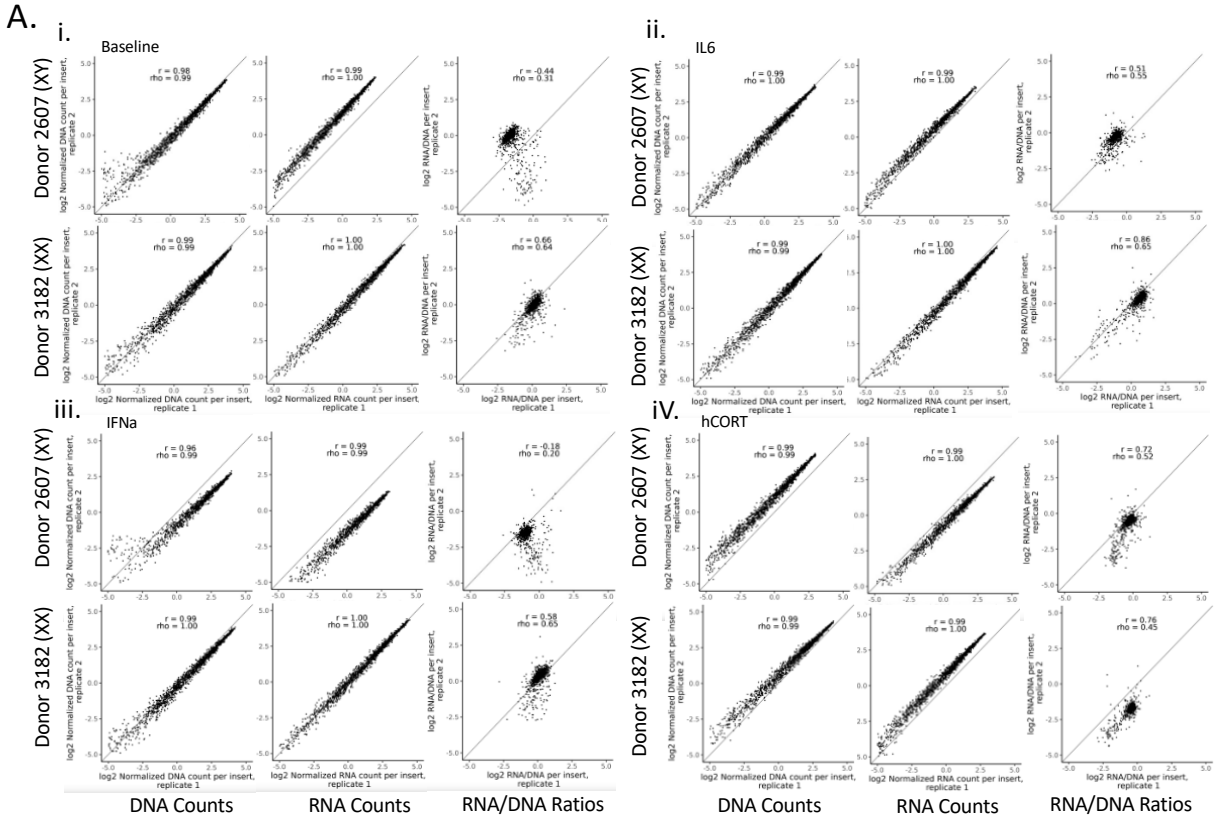

Supplemental Figure 12. Correlation between MPRA experimental replicates. The normalized log2 DNA and RNA counts per CRE are strongly correlated between replicates (Pearson's rho-correlation 0.98-1.00) for each MPRA. Transcriptional activity, measured as the log2 normalized RNA/DNA ratios, is moderately to strongly correlated between replicates (rho=0.20-0.65).

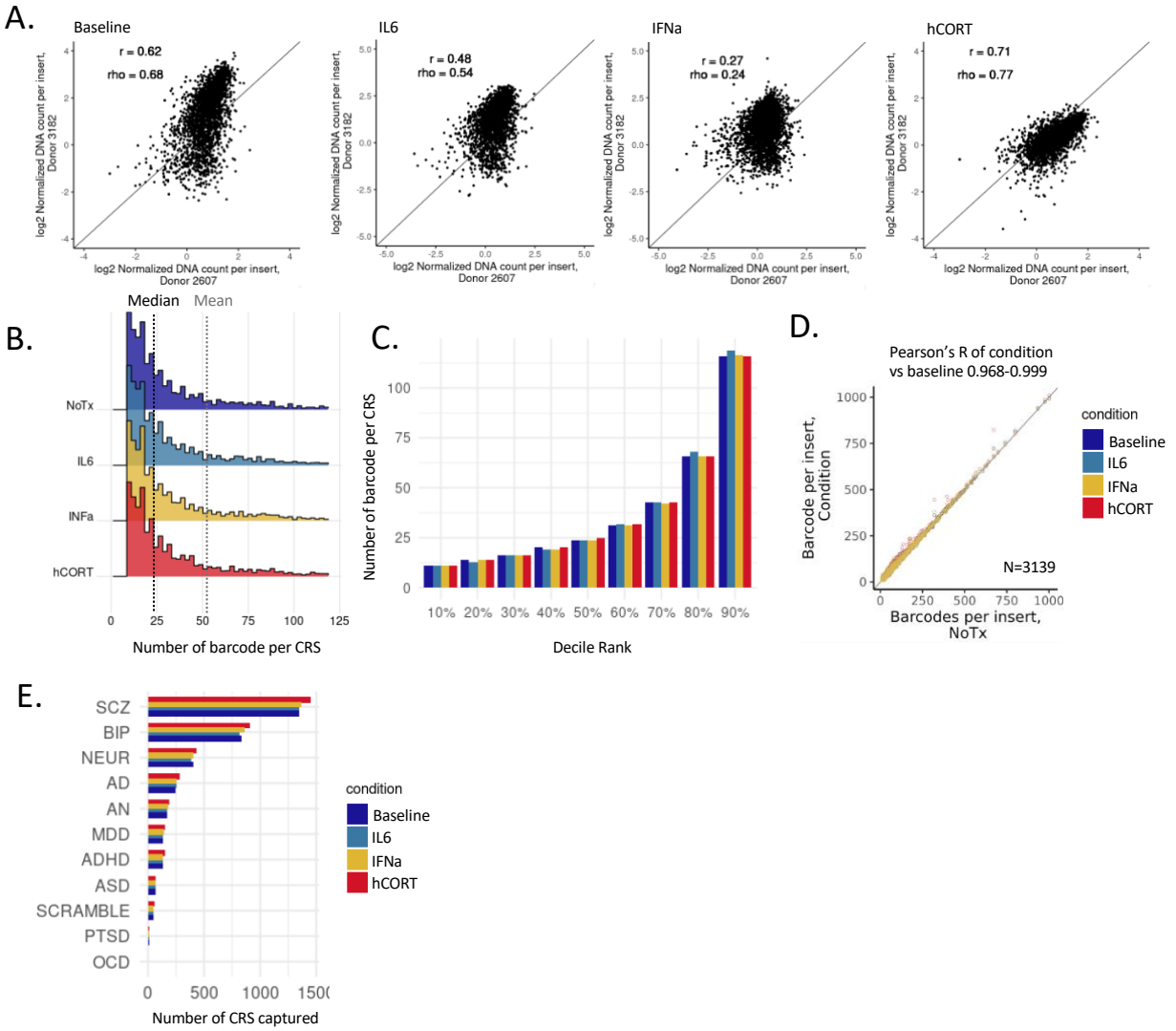

Supplemental Figure 13. Correlation between MPRA donors and contexts. (**A**) Transcriptional activity, measured as the log2 normalized RNA/DNA ratios, is strongly correlated between donors (rho=0.54-0.77) and moderately correlated following IFNa exposure (rho=0.24). Across conditions 3,440-3747 of CRE were captured (minimum requirement of 10 barcodes each) and the number of barcodes per unique CRE were highly correlated between CRE shared across all conditions (rho 0.968-0.999; nCRE=3139) (**B-D**). There was no significant difference in mean number of barcodes per insert or the proportion of CRE by prioritization method or disorder association across the conditions (**E**). There were no significant differences in the number of captured CRE by disorder across MPRAs.

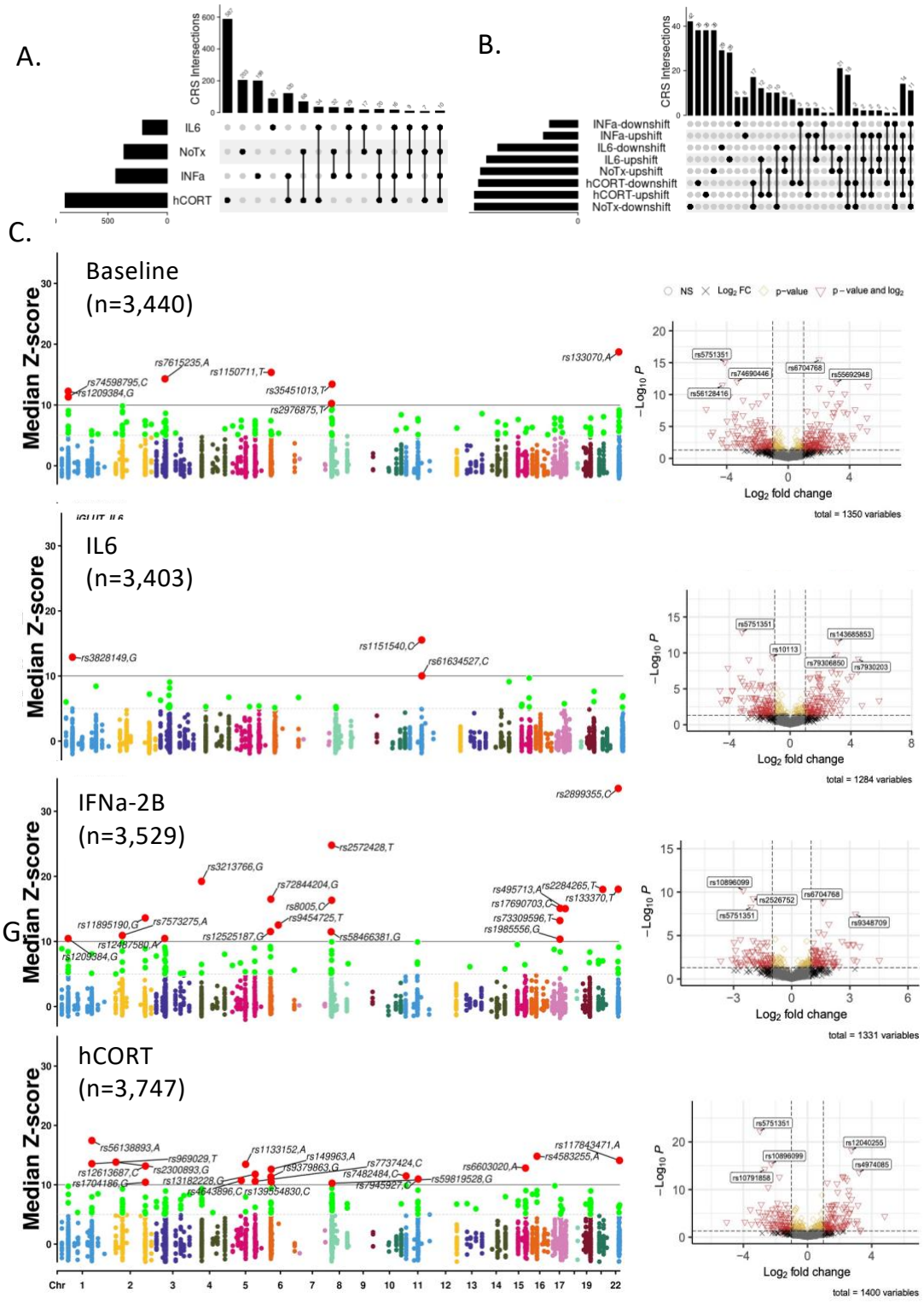

Supplemental Figure 14. **Stress and inflammatory factors uniquely impacted allelic-specific transcriptional activity of CRE in neurons. (A)** Overlap of active enhancers (FDR<=0.1) across conditions. **(B)** Overlap of allelic shifts across conditions. **(C)** Manhattan plots of differentially active CRE across cues labeled by SNP and variant with chromosomal location

on the x-axis and the median transcriptional activity compared to scramble controls on the y-axis. Comparative volcano plots showing cue-specific CRE compared to baseline (related to **Figure 2**)**.**

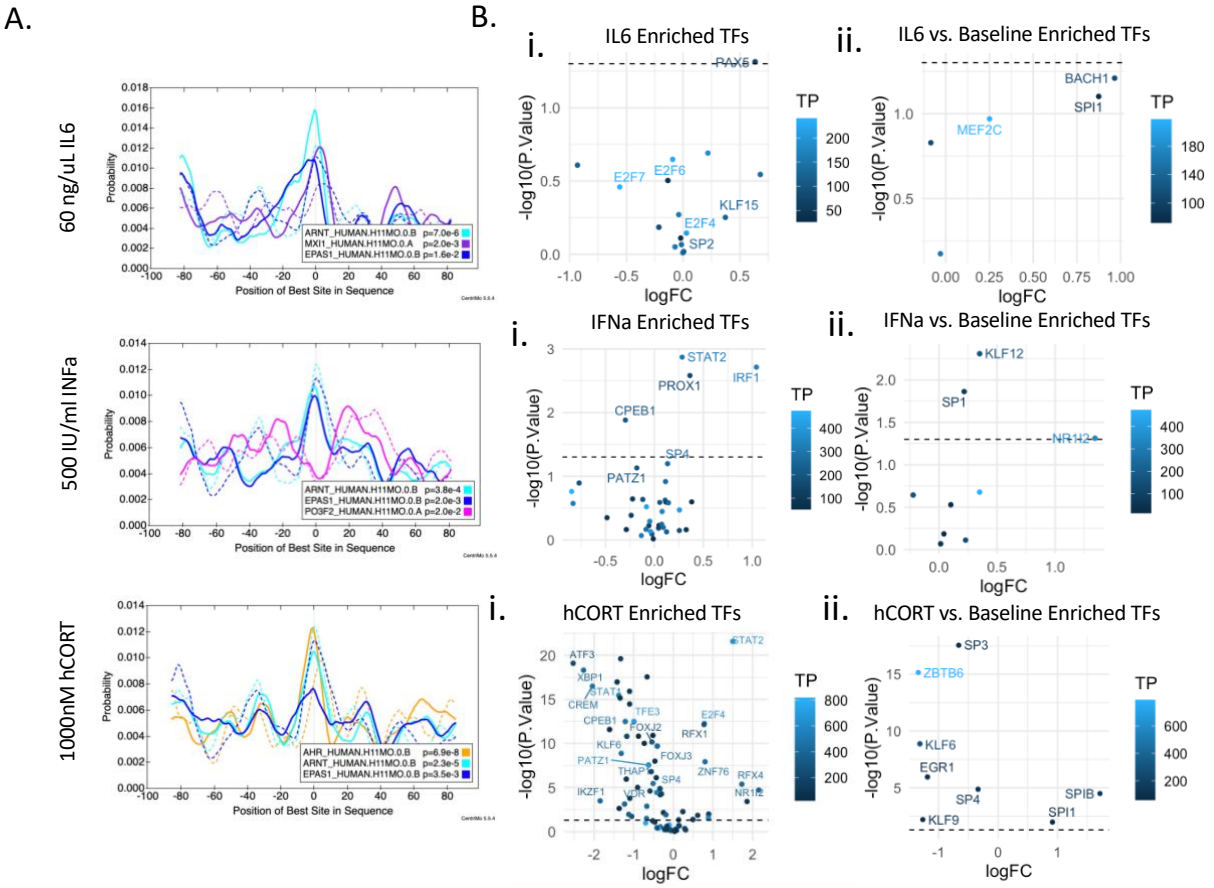

C.

TF	Motif	GWAS associations
ARNT		SCZ, Alzheimer's Disease
EPAS1		COVID-19, Asthma, impulse control disorder
MXI1		Multiple sclerosis, Bipolar Disorder
POU3F2		ASD, ADHD, BIP, SCZ, suicide, neuroticism
AHR		Parkinson disease, Crohn's disease, psoriasis, Ulcerative Colitis

D.

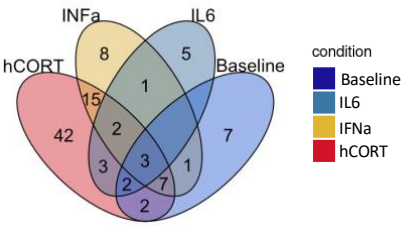

Supplemental Figure 8. Transcription factor binding motifs were differentially enriched in active CRE based on context. (A) Differential transcription factor motif enrichment analyses centered at the tested SNP (MEME Suite, CentriMO) identified cue-specific and shared TFs. **(B)** Filtering for TFs that are expressed in iGLUTs, motif enrichment analysis without bias for the center of the CRE of core TF motifs (HOCOMOCO v11) identified significantly active CRE across exposures that demonstrate shared and unique enrichments. TFs targeting enriched motifs were uniquely differentially expressed following cue exposure. **(C)** TFs of motifs enriched at the

sequence center had known GWAS associations listed on GeneCards. **(D)** Overlap of motif enrichments by cue identify only 3 shared TF enrichments (related to **Figure 4**)**.**

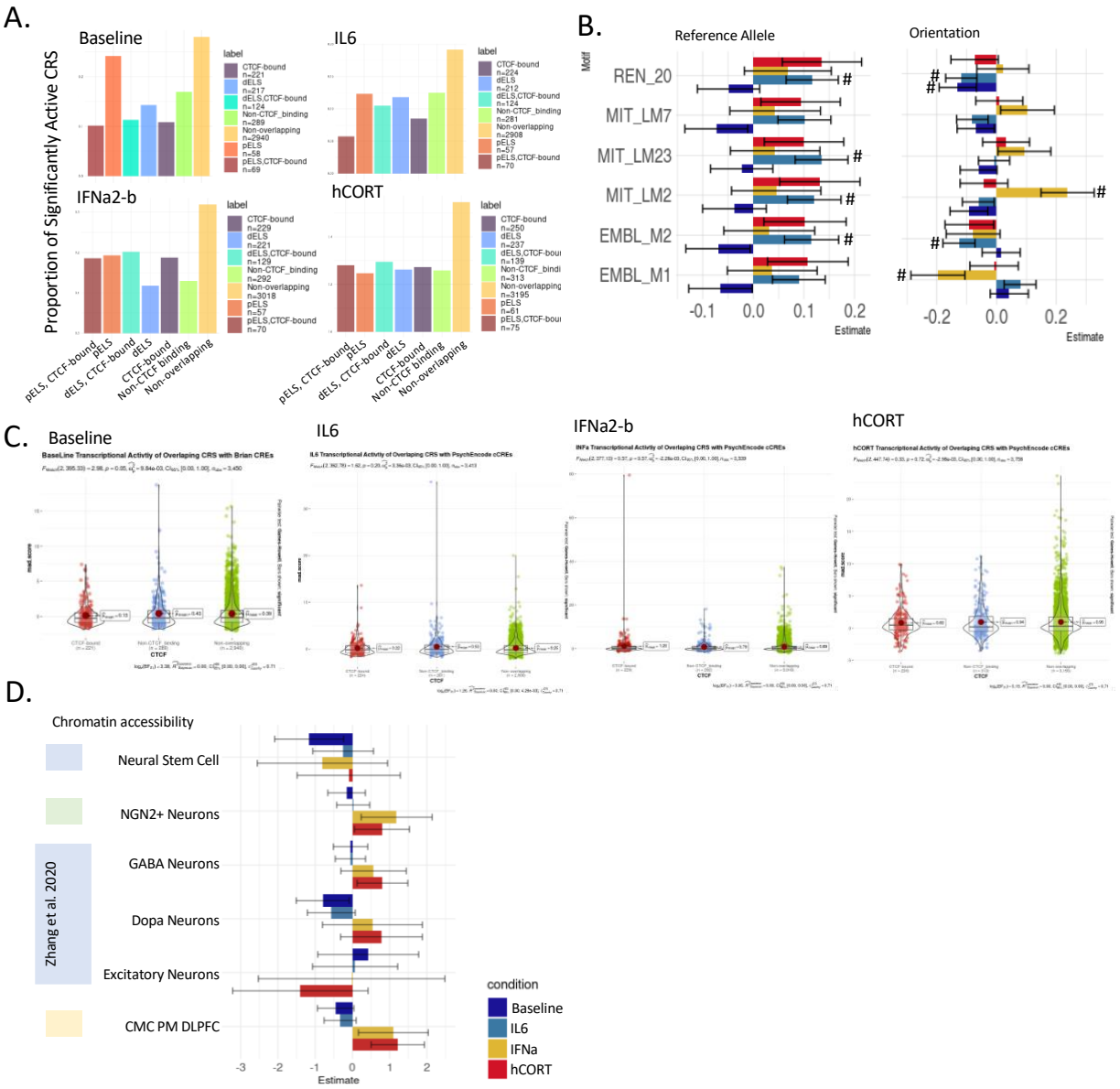

Supplemental Figure 9. CTCF binding, but not chromatic accessibility measures, influenced cue-specific MPRA allelic shifts. (A) The proportion of significantly active CRE overlapping with known proximal or distal enhancer or promoter like sequences from ENCODE cCRE annotations shifted with exposure to stress and inflammatory factors. **(B)** Estimates for impact of allele and orientation matched to (related to **Figure 2-B,i-iv);** (MPRA median z-score ~ CTCF motif score + orientation + allele + distance from center SNP + motif). **(C)** At baseline, the average activity of CTCF-bound sequences is significantly lower compared to non CTCF-bound regions, but not following stress and inflammation. **(D)** Chromatin accessibility peaks across studies do not predict CRE activity (**Supplemental Data 1**).

1287

A.

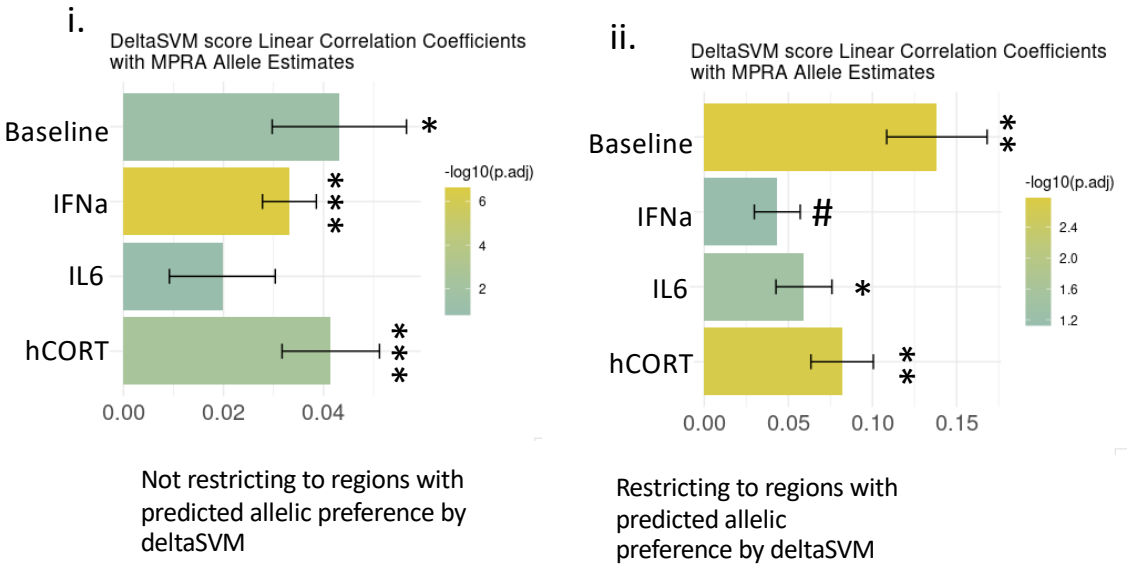

Allelic effect * -log10(pvalue) ~ deltaSVMscore + TF

B.

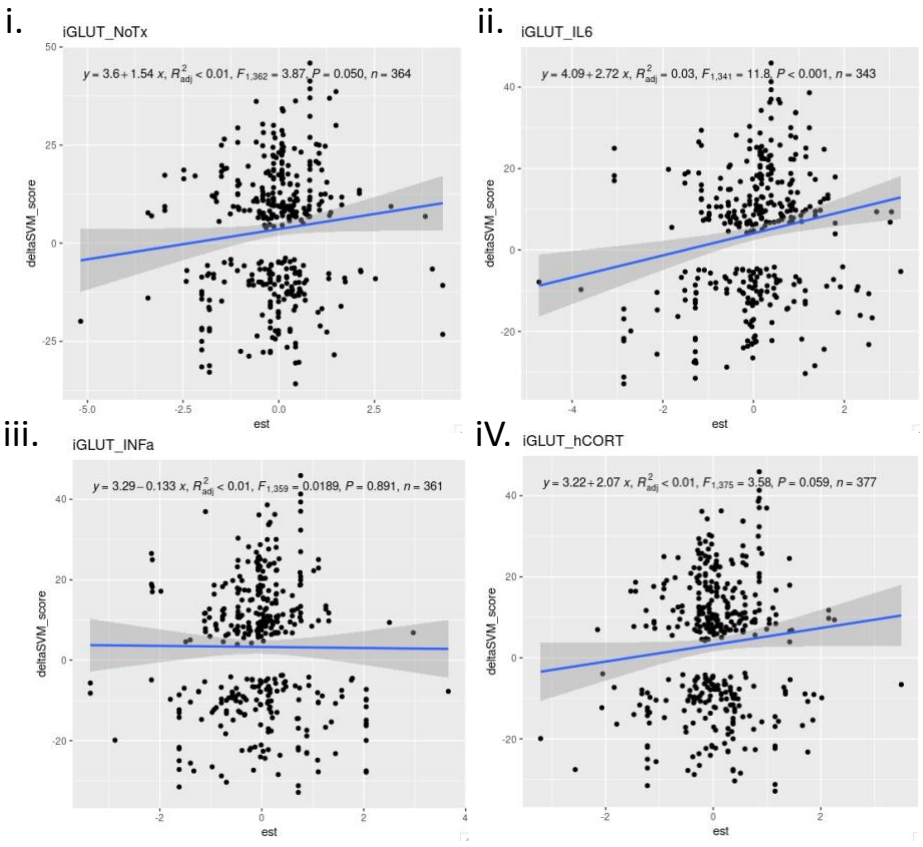

1288

1289 **Supplemental Figure 10. Predicted TF binding SNP regulatory effects correlated**
1290 **significantly with MPRA allelic shifts. (A)** (i) Linear correlation coefficients without filtering for
1291 evidence of strong allelic preference by deltaSVM and (ii) after filtering for strong allelic preference

by deltaSVM. Correlation plots of deltaSVM score by MPRA measured cue-by-variant shifts. Allelic effect * -log(pvalue) ~ deltaSVMscore + TF. (FDR<=0.08$^{\#}$, FDR<0.05*,FDR<0.01**,FDR<0.001***). **(B)** Scatter plots of baseline (i), hCort-responsive (ii), IFNa-responsive (iii), hCort-responsive (iv) allele specific MPRA activity (x-axis) and CRE deltaSVM scores based on TF binding affinities with linear modeling (related to **Figure 5, SI Figure 11**)**.**

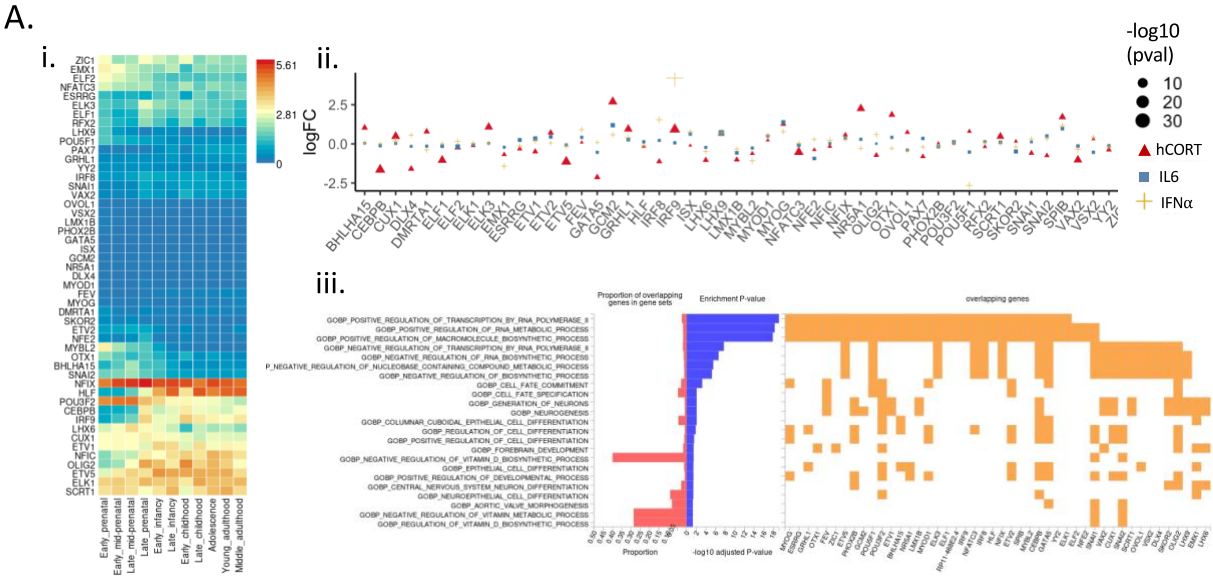

Supplemental Figure 11. Expression of TFs predicted to regulate cue-specific MPRA activity. (A) Transcription factors with binding affinities that significantly predict MPRA activity (related to **Figure 5, SI Figure 10; Supplemental Data 2**) are differentially expressed across development in the human brain **(i)**, are differentially expressed in DIV24 iGLUTs following exposure to 60ng/uL IL-6, 500 IU/mL IFNa, and 1000nM hCort **(ii)**, and are enriched for neurogenesis and neuron development by FUMA **(iii)**.

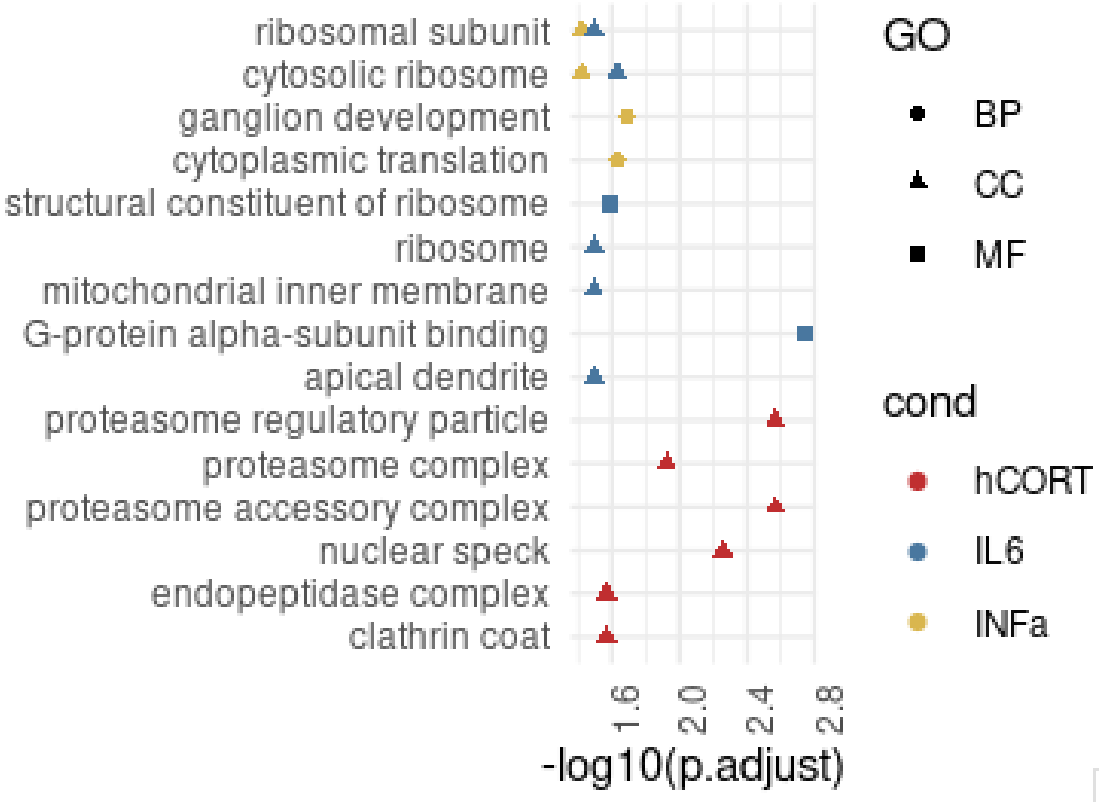

Supplemental Figure 12. Cue-specific impacts on biological pathways. (A) Biological theme comparison identifies IFNa pathways that are differentially enriched between ABC genes predicted by cue-specific MPRA activity and chromatin accessibility (related to **Figure 6**).